Earthq Eng & Eng Vib (2017) 16: 131-152 **DOI**: 10.1007/s11803-017-0373-1

A new methodology for energy-based seismic design of steel moment frames

Mebrahtom Gebrekirstos Mezgebo[1†] and Eric M. Lui[2‡]

1. *Michael Baker International, Hamilton, NJ 08619, USA*

2. *Department of Civil and Environmental Engineering, Syracuse University, Syracuse, NY 13244-1240, USA*

Abstract: A procedure is proposed whereby input and hysteretic energy spectra developed for single-degree-of-freedom (SDOF) systems are applied to multi-degree-of-freedom (MDOF) steel moment resisting frames. The proposed procedure is verified using four frames, viz., frame with three-, five-, seven- and nine-stories, each of which is subjected to the fault-normal and fault-parallel components of three actual earthquakes. A very good estimate for the three- and five-story frames, and a reasonably acceptable estimate for the seven-, and nine-story frames, have been obtained. A method for distributing the hysteretic energy over the frame height is also proposed. This distribution scheme allows for the determination of the energy demand component of a proposed energy-based seismic design (EBSD) procedure for each story. To address the capacity component of EBSD, a story-wise optimization design procedure is developed by utilizing the energy dissipating capacity from plastic hinge formation/rotation for these moment frames. The proposed EBSD procedure is demonstrated in the design of a three-story one-bay steel moment frame.

Keywords: energy-based seismic design; hysteretic energy distribution; MDOF systems; steel moment frames; story-wise optimization design

1 Introduction

Like any earthquake spectrum, input and hysteretic energy spectra are derived from single degree-of-freedom (SDOF) systems. Since most structures in reality are multi-degree-of-freedom (MDOF) systems, a methodology for estimating input and hysteretic energy demands for MDOF systems using information from single-degree-of-freedom (SDOF) systems is needed. Furthermore, for the purpose of design an energy distribution scheme is needed to apportion the total system hysteretic energy to each part of a MDOF structure.

In this paper, a methodology to extend the energy demands from a SDOF system to a MDOF system is proposed. An energy distribution scheme that can be used for the design of multi-story steel moment frames is also proposed. In addition, a story-wise optimization design procedure for steel moment resisting frames is developed by utilizing their energy dissipating capacity from plastic hinge formation/rotation.

Correspondence to: Eric M. Lui, Department of Civil and Environmental Engineering, Syracuse University, USA
Tel: +1-315-443-3394; Fax: +1-315-443-1243
E-mail: emlui@syr.edu
[†]Structural Engineer; [‡]Meredith Professor

Received September 8, 2015; **Accepted** March 20, 2016

Regardless of the size of the structure or whether it is a SDOF or MDOF system, the first step in energy-based seismic design (EBSD) is to determine the seismic energy demand on the structure due to the design earthquake. Seismic energy demand or hysteretic energy is the inelastic component of the absorbed energy of the total seismic input energy imparted to a structure and it is a function of the hysteretic behavior of the structure. For a given design earthquake, structures of equal weight/mass but have different hysteretic behavior will experience different seismic energy demands. Expectedly, different seismic energy demands will require different energy dissipation capacities. In EBSD, the structure has to be designed so its energy dissipation capacity will exceed the energy demand. The fact that almost all practical structures are MDOF systems means one needs to go beyond SDOF systems and study the seismic input and hysteretic energy of MDOF systems. Compared to SDOF systems, the determination of seismic energy demand for MDOF systems is understandably more difficult. The number of dynamic equations involved along with the potential coupling effect of different responses makes the determination of seismic input energy and the accompanying hysteretic energy in MDOF systems rather difficult. However, using SDOF systems as the basis, research has shown that the input energy for MDOF structures can be obtained in an

approximate manner.

Akiyama (1985) used the S00E component of the 1940 El Centro record to compute the input energy using a Fourier Spectra for a five-story building. He compared it with the input energy of an equivalent one-story building having the same fundamental period of vibration, total mass, and yield strength, and concluded that the input energy for the MDOF structure could be estimated from the input energy of the equivalent SDOF system. He also reported that the parameters that affected earthquake input energy were mainly the mass and period of the structure. Nakashima *et al*. (1996), in their study on the energy behavior of structures with hysteretic dampers, found that the total input energy and hysteretic energy for MDOF systems were approximately the same as those of the equivalent SDOF systems. They also found that this was true even for a large value of post-to-pre-yield stiffness ratio. The effect of post-to-pre-yield stiffness ratio was only important on the distribution of hysteretic energy at different levels of the structure.

Shen and Akbas (1999) computed earthquake input energy for a three-, six- and ten-story moment resisting steel frames using equivalent SDOF systems. They compared the input energy expressions formulated based on the energy balance equation and empirical equations by Housner (1956), Akiyama (1985), Fajfar *et al*. (1989), Kuwamura and Galambos (1989) and Uang and Bertero (1990) and found that energies for MDOF and the corresponding equivalent SDOF structures were significantly different since the empirical equations did not take into account structural properties such as period of vibration and hysteretic behavior.

Chou and Uang (2003) developed an empirical formula to estimate the absorbed energy in multistory fames using an energy spectra developed for SDOF systems. They used a static pushover analysis to determine the yield force and ductility factor of an equivalent SDOF system. For low-to-medium rise buildings, they showed that by using just two modes of the MDOF systems their empirical formula could be used to estimate the absorbed energy in MDOF systems from the equivalent SDOF systems. Li *et al*. (2007) and Ye *et al*. (2009) also proposed procedures for obtaining hysteretic energy of MDOF structures from equivalent SDOF structures. Their procedures take into account only the first mode of the MDOF structures. Using eight examples (two regular and six irregular MDOF structures), they concluded that their procedure was an effective and simple way of obtaining the hysteretic energy demands of MDOF structures. Ye *et al*. (2009) also studied the energy-based seismic design and its application for steel braced frame structures, and proposed an inelastic input energy spectrum for SDOF structures together with a relationship between hysteretic energy and input energy. They concluded that the input energy for MDOF structures could be estimated from the equivalent SDOF structures. For structures in the moderate and long period regions, they proposed expressions to estimate the input energy for MDOF systems from their equivalent SDOF systems as well as presented equations for the ratio of hysteretic-to-input energy for MDOF structures.

In this study, an equation that relates the energy demand of a MDOF system and the corresponding SDOF systems is formulated and proposed. An energy distribution scheme is then developed to allow for the allocation of this energy demand to each story of a steel moment resisting frame. A story-wise design procedure suitable for use in an EBSD of these frames is then introduced.

2 Equivalent SDOF systems

The equations of motion for a MDOF system with n degrees of freedom subjected to earthquake ground acceleration $\ddot{u}_g(t)$ can be expressed as

$$\boldsymbol{M}\ddot{\boldsymbol{u}}(t)+\boldsymbol{C}\dot{\boldsymbol{u}}(t)+\tilde{\boldsymbol{K}}\boldsymbol{u}(t)=-\boldsymbol{M}\boldsymbol{\iota}\ddot{u}_g(t) \tag{1}$$

where $\boldsymbol{M},\boldsymbol{C},\tilde{\boldsymbol{K}}$ are the mass, damping and stiffness matrices of size ($n \times n$), respectively; $\ddot{\boldsymbol{u}}(t)$, $\dot{\boldsymbol{u}}(t)$, $\boldsymbol{u}(t)$ are the relative acceleration, velocity and displacement vectors of the n-degrees of freedom system, respectively; and $\boldsymbol{\iota}$ is the influence vector that accounts for the effect of ground excitation on a specific degree of freedom of the structure (Chopra, 2012).

If we denote $\boldsymbol{u}(t)=\boldsymbol{\Phi}\boldsymbol{x}(t)=\sum_{i=1}^{n}\boldsymbol{\phi}_i x_i(t)$ where $\boldsymbol{\Phi}$ is the $n \times n$ mode shape matrix composed of n mode shape vectors $\boldsymbol{\phi}_i$, each of dimension $n \times 1$, and is the modal displacement vector composed of modal displacements $x_i(t)$, $i = 1,2,\ldots n$, then upon substituting the terms for $\boldsymbol{u}(t)$, Eq. (1) can be written as

$$\boldsymbol{M}\sum_{i=1}^{n}\boldsymbol{\phi}_i\ddot{x}_i(t)+\boldsymbol{C}\sum_{i=1}^{n}\boldsymbol{\phi}_i\dot{x}_i(t)+\tilde{\boldsymbol{K}}\sum_{i=1}^{n}\boldsymbol{\phi}_i x_i(t)=-\boldsymbol{M}\boldsymbol{\iota}\ddot{u}_g(t) \tag{2}$$

For Mode r, multiplying both sides of the above equation by $\boldsymbol{\phi}_r^{\mathrm{T}}$ gives

$$\boldsymbol{\phi}_r^{\mathrm{T}}\boldsymbol{M}\sum_{i=1}^{n}\boldsymbol{\phi}_i\ddot{x}_i(t)+\boldsymbol{\phi}_r^{\mathrm{T}}\boldsymbol{C}\sum_{i=1}^{n}\boldsymbol{\phi}_i\dot{x}_i(t)+\boldsymbol{\phi}_r^{\mathrm{T}}\tilde{\boldsymbol{K}}\sum_{i=1}^{n}\boldsymbol{\phi}_i x_i(t)=-\boldsymbol{\phi}_r^{\mathrm{T}}\boldsymbol{M}\boldsymbol{\iota}\ddot{u}_g(t) \tag{3}$$

In nonlinear analysis, responses in different modes are often coupled. However, in modal analysis, responses in different modes are assumed to be independent. Although theoretically incorrect, the assumption of modal independence has been used for nonlinear analysis of systems with material nonlinearity by a number of researchers. Chopra and Goel (2002), Chou and Uang (2003), Hernandes-Montes *et al*. (2004) and Prasanth *et al.* (2008) have all applied this assumption

in determining seismic demand for buildings and found that the assumption was acceptable. As a result, the present study will assume that the different modes are uncoupled and are orthogonal to one another. By using this assumption and by assuming classical damping for the system, Eq. (3) can now be written for any mode *r* of a MDOF system as

$$\boldsymbol{\phi}_r^{\mathrm{T}}\boldsymbol{M}\boldsymbol{\phi}_r\ddot{x}_r(t)+\boldsymbol{\phi}_r^{\mathrm{T}}\boldsymbol{C}\boldsymbol{\phi}_r\dot{x}_r(t)+\boldsymbol{\phi}_r^{\mathrm{T}}\tilde{\boldsymbol{K}}\boldsymbol{\phi}_r x_r(t)=-\boldsymbol{\phi}_r^{\mathrm{T}}\boldsymbol{M}\boldsymbol{\iota}\ddot{u}_{\mathrm{g}}(t) \quad (4)$$

Defining $\boldsymbol{\phi}_r^{\mathrm{T}}\boldsymbol{M}\boldsymbol{\phi}_r=M_r$ and $\boldsymbol{\phi}_r^{\mathrm{T}}\boldsymbol{C}\boldsymbol{\phi}_r=C_r$, and substituting these equations in Eq. (4) yields

$$M_r\ddot{x}_r(t)+C_r\dot{x}_r(t)+\boldsymbol{\phi}_r^{\mathrm{T}}\tilde{\boldsymbol{K}}\boldsymbol{\phi}_r x_r(t)=-\boldsymbol{\phi}_r^{\mathrm{T}}\boldsymbol{M}\boldsymbol{\iota}\ddot{u}_{\mathrm{g}}(t) \quad (5)$$

Dividing both sides of Eq. (5) by M_r, and defining a modal participation factor for Mode *r* as $\Gamma_r=\dfrac{\boldsymbol{\phi}_r^{\mathrm{T}}\boldsymbol{M}\boldsymbol{\iota}}{M_r}=\dfrac{L_r}{M_r}$, and a nonlinear stiffness–displacement relationship as $\boldsymbol{\phi}_r^{\mathrm{T}}\tilde{\boldsymbol{K}}\boldsymbol{\phi}_r x_r(t)=F_r(t)$, the above equation can be written as

$$\ddot{x}_r(t)+2\zeta_r\omega_r\dot{x}_r(t)+\frac{F_r(t)}{M_r}=-\Gamma_r\ddot{u}_{\mathrm{g}}(t) \quad (6)$$

If the modal displacement is redefined as $x_r(t)=\Gamma_r D_r(t)$ where $D_r(t)$ is a generalized displacement for mode *r*, Eq. (6) becomes

$$\ddot{D}_r(t)+2\zeta_r\omega_r\dot{D}_r(t)+\frac{F_r(t)}{L_r}=-\ddot{u}_{\mathrm{g}}(t) \quad (7)$$

Equation (7) can be interpreted as the governing equation for the *r*th- mode inelastic SDOF with initial natural frequency ω_r and damping ratio ζ_r for the *r*th-mode linear MDOF system (Chopra and Goel, 2002). The equation can be conveniently solved by standard software as it is similar to a standard equation of motion of a SDOF system.

The properties of the *r*th-mode inelastic SDOF system are determined using a pushover curve obtained from a nonlinear static analysis of the MDOF structure pushed to some predetermined displacement using a lateral force distribution given by $\boldsymbol{S}_r = \boldsymbol{M}\boldsymbol{\phi}_r$. The force distribution is set to be proportional to the mode shape $\boldsymbol{\phi}_r$ of the MDOF system. In a classical pushover analysis, the roof displacement is considered to be a representative response and is taken as a predetermined target displacement to which the structure is pushed. However, it is important to note that some researchers, e.g., Manoukas *et al.* (2011), have proposed energy-based static pushover analysis procedures where the predetermined displacement will be independent of any particular story displacement but a displacement pertinent to the energy.

Generally, the base shear V_{br} versus roof displacement u_{tr} plot obtained from a pushover analysis of a MDOF system is converted into an $\dfrac{F_r}{L_r}$ versus D_r plot of an equivalent SDOF system. The relationships between (V_{br}, u_{tr}) of the MDOF system pushover curve and ($\dfrac{F_r}{L_r}$, D_r) of the equivalent SDOF system are given by Chopra (2012) as

$$\frac{F_r}{L_r}=\frac{V_{br}}{M_r^*}=\frac{V_{br}}{L_r\Gamma_r};\quad D_r=\frac{u_{tr}}{\Gamma_r\phi_{tr}} \quad (8a,b)$$

where $M_r^*=L_r\Gamma_r$ is the mass participation factor or effective modal mass for Mode *r*.

Figure 1(a) shows a typical actual and idealized pushover curve obtained from a pushover analysis of a MDOF system pushed to a predetermined roof displacement using a lateral force distribution specified for Mode Shape *r*. Figure 1(b) is a force-displacement relationship for the *r*th mode of an equivalent inelastic SDOF system generated from the actual pushover curve of Fig. 1(a). The properties of the equivalent inelastic SDOF (α_r, ω_r, D_{ry}) are used in Eq. (7) for the analysis of the equivalent SDOF system.

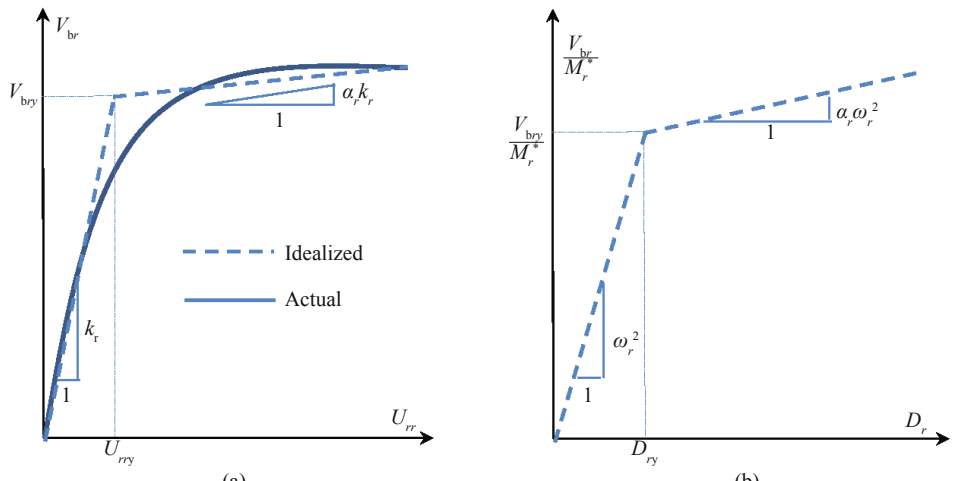

Fig. 1 (a) Pushover curve for the *r*th mode of a MDOF system; (b) Force-deformation relation for the corresponding inelastic equivalent SDOF system

3 Energy balance for MDOF systems

The energy balance equation for a MDOF system can be written as

$$\int_0^t \boldsymbol{M}\ddot{\boldsymbol{u}}(t)\,\dot{\boldsymbol{u}}(t)\mathrm{d}\tau + \int_0^t \boldsymbol{C}\dot{\boldsymbol{u}}(t)\,\dot{\boldsymbol{u}}(t)\mathrm{d}\tau + \int_0^t \tilde{\boldsymbol{K}}\boldsymbol{u}(t)\,\dot{\boldsymbol{u}}(t)\mathrm{d}\tau = \int_0^t -\boldsymbol{M}\boldsymbol{\iota}\ddot{u}_{\mathrm{g}}(t)\,\dot{\boldsymbol{u}}(t)\mathrm{d}\tau \tag{9}$$

or

$$E_{\mathrm{kr}} + E_{\mathrm{d}} + E_{\mathrm{a}} = E_i \tag{10}$$

where

$$E_{\mathrm{kr}} = \text{relative kinetic energy} = \int_0^t \boldsymbol{M}\ddot{\boldsymbol{u}}(t)\,\dot{\boldsymbol{u}}(t)\mathrm{d}\tau \tag{11}$$

$$E_{\mathrm{d}} = \text{damping energy} = \int_0^t \boldsymbol{C}\dot{\boldsymbol{u}}(t)\,\dot{\boldsymbol{u}}(t)\mathrm{d}\tau \tag{12}$$

$$E_{\mathrm{a}} = \text{absorbed energy} = \int_0^t \tilde{\boldsymbol{K}}\boldsymbol{u}(t)\,\dot{\boldsymbol{u}}(t)\mathrm{d}\tau \tag{13}$$

$$\mathrm{IE} = \text{relative input energy} = \int_0^t -\boldsymbol{M}\boldsymbol{\iota}\ddot{u}_{\mathrm{g}}(t)\,\dot{\boldsymbol{u}}(t)\mathrm{d}\tau \tag{14}$$

For Mode r with the modal equation of motion given in Eq. (5), the modal energy balance equation can be expressed as

$$\int_0^t M_r\ddot{x}_r(t)\dot{x}_r(t)\mathrm{d}\tau + \int_0^t C_r\dot{x}_r(t)\dot{x}_r(t)\boldsymbol{d}\tau + \int_0^t \boldsymbol{\phi}_r^{\mathrm{T}}\tilde{\boldsymbol{K}}\boldsymbol{\phi}_r x_r(t)\dot{x}_r(t)\mathrm{d}\tau = \int_0^t -\boldsymbol{\phi}_r^{\mathrm{T}}\boldsymbol{M}\boldsymbol{\iota}\ddot{u}_{\mathrm{g}}(t)\dot{x}_r(t)\mathrm{d}\tau \tag{15}$$

or

$$E_{\mathrm{kr}}^r + E_{\mathrm{d}}^r + E_{\mathrm{a}}^r = \mathrm{IE}^r \tag{16}$$

where $E_{\mathrm{kr}}^r, E_{\mathrm{d}}^r, E_{\mathrm{a}}^r, \mathrm{IE}^r$ are the relative kinetic energy, damping energy, absorbed energy and input energy contributions by Mode r to the MDOF system, respectively.

Since Eq. (7) is the equation of motion of a SDOF with unit mass that corresponds to Mode r of the MDOF system, the absorbed and input energy per unit mass for this equivalent SDOF system are therefore

$$\frac{E_{a,\mathrm{SDOF}}^r}{m} = \int_0^t \frac{F_r(t)}{L_r}\dot{D}_r(t)\mathrm{d}\tau \quad \text{and} \quad \frac{\mathrm{IE}_{\mathrm{SDOF}}^r}{m} = \int_0^t -\ddot{u}_{\mathrm{g}}(t)\dot{D}_r(t)\mathrm{d}\tau \tag{17a,b}$$

Because $x_r(t) = \Gamma_r D_r(t)$, $F_r(t) = \boldsymbol{\phi}_r^{\mathrm{T}}\tilde{\boldsymbol{K}}\boldsymbol{\phi}_r x_r(t)$, $L_r = \boldsymbol{\phi}_r^{\mathrm{T}}\boldsymbol{M}\boldsymbol{\iota}$ and $M_r^* = L_r\Gamma_r$, the above equations can be written as

$$\frac{E_{a,\mathrm{SDOF}}^r}{m} = \int_0^t \frac{F_r(t)}{L_r}\dot{D}_r(t)\mathrm{d}\tau = \frac{1}{L_r\Gamma_r}\int_0^t \boldsymbol{\phi}_r^{\mathrm{T}}\tilde{\boldsymbol{K}}\boldsymbol{\phi}_r x_r(t)\dot{x}_r(t)\mathrm{d}\tau = \frac{1}{M_r^*}E_a^r \tag{18a}$$

$$\frac{IE_{\mathrm{SDOF}}^r}{m} = \int_0^t -\ddot{u}_{\mathrm{g}}(t)\dot{D}_r(t)\mathrm{d}\tau = \frac{1}{L_r\Gamma_r}\int_0^t -\boldsymbol{\phi}_r^{\mathrm{T}}\boldsymbol{M}\boldsymbol{\iota}\ddot{u}_{\mathrm{g}}(t)\dot{x}_r(t)\mathrm{d}\tau = \frac{1}{M_r^*}\mathrm{IE}^r \tag{18b}$$

In the event that the mode shapes are mass normalized, $M_r = 1$ and so Γ_r is numerically equal to L_r, the above equations can be written as

$$\frac{E_{a,\mathrm{SDOF}}^r}{m} = \frac{1}{(\Gamma_r)^2}E_a^r \quad \text{and} \quad \frac{\mathrm{IE}_{\mathrm{SDOF}}^r}{m} = \frac{1}{(\Gamma_r)^2}\mathrm{IE}^r \tag{19a,b}$$

Equations (18a), (18b); or Eqs. (19a), (19b) if the mode shapes are mass normalized; are the absorbed and input energy equations that relate the rth mode of the MDOF system with its equivalent SDOF system with properties described by Eqs. (8a), (8b). The amount of input and absorbed energies of a MDOF system obtained using these mode-based relationships is dependent on the modal characteristics of the MDOF system besides the seismicity of the site.

4 Estimating hysteretic and input energies for MDOF systems

The proposed modal-based procedure for estimating the input and hysteretic energies for a MDOF structure from its modal SDOF structures is outlined below:

(1) Estimate the initial periods of vibration for the MDOF structure and the corresponding effective modal masses.

(2) Determine the number of modes to be used so that the sum of effective modal masses considered is ≥ 90% of the total mass of the structure as recommended by FEMA 273 (1997).

(3) For each mode, generate pushover curve by pushing the MDOF structure with a lateral load pattern that matches the respective mode shape.

(4) For each mode, use the expressions given in Eqs. (8a,b) to develop a force-displacement relationship for an inelastic equivalent SDOF system from the modal pushover curve of the MDOF system.

(5) From the resulting pushover force-displacement curve, determine the yield force, initial stiffness and post-yield stiffness ratio for each mode.

(6) Using the yield force, initial stiffness and post-yield stiffness ratio for each mode, determine the corresponding ductility factor. The ductility factor can be determined using one of the following approaches

(a) by time history analysis of the SDOF for a given earthquake, or

(b) from a ductility-based yield force spectra if readily available, or

(c) from a prescribed desired ductility level

Options (a) or (b) is used if the main objective is to determine the energy capacity of an MDOF systems, whereas option (c) is used if the objective is to design an energy dissipating mechanism for a MDOF system.

(7) Using the ductility factor and period of vibration, obtain the input and hysteretic energies for each mode from the input and hysteretic energy spectra developed for SDOF systems.

(8) The input and hysteretic energies of the MDOF structure are then computed using the following equations

$$\mathrm{IE}_{\mathrm{MDOF}} = \sum_{r=1}^{n_m} (M_r^* \times \frac{\mathrm{IE}_{\mathrm{SDOF}}^r}{m}) \qquad \mathrm{HE}_{\mathrm{MDOF}} = \sum_{r=1}^{n_m} (M_r^* \times \frac{\mathrm{HE}_{\mathrm{SDOF}}^r}{m}) \tag{20a,b}$$

where

M_r^* = mass participation factor for mode r

m = system mass

n_m = number of modes considered

$\mathrm{IE}_{\mathrm{MDOF}}$ = estimated input energy for the MDOF system

$\mathrm{HE}_{\mathrm{MDOF}}$ = estimated hysteretic energy for the MDOF system

$\mathrm{IE}^r_{\mathrm{SDOF}}/m$ = input energy per unit mass of the SDOF system for Mode r

$\mathrm{HE}^r_{\mathrm{SDOF}}/m$ = hysteretic energy per unit mass of the SDOF system for Mode r

5 Verification study

The ability of Eq. (20a) to estimate input energy for MDOF structures from the input energy equations for SDOF systems is demonstrated using four moment resisting frames with 3-, 5-, 7- and 9-stories. These moment resisting frames have been used previously by researchers such as Gupta and Krawinkler (1999), Chou and Uang (2003) and Prasanth *et al*. (2008) and frame details can be found in these references. The design parameters used for and the design procedures involved in the design of these ductile moment resisting frames can be found in Chou (2001). The 9-story building has steel moment resisting frames in both directions and was designed by a SAC commissioned consulting firm based on the procedures of UBC (1997). The 3-story and 9-story buildings were composed of steel columns and beams whereas the 5-story and 7-story buildings were designed using steel encased reinforced concrete (SRC) columns and steel beams. For the 3-, 5- and 7-story frames, a reduced beam section with 50% reduction in both the top and bottom flanges was used to reduce the demand to the connections. Other than at the base of the columns, this ensures that hinges do form first at beam ends for a given connection.

To determine the number of modes to be used in the analysis, the recommendation by FEMA 273 (1997) that the sum of the effective modal masses considered is ≥ 90% of the total mass of the structure is used. As shown in Table 1, two modes are considered sufficient for the present study.

Static pushover analysis results for the first and second modes of these frames are shown in Figs. 2(a) and 2(b), respectively. The static pushover analyses were obtained by subjecting the frames to a pattern of lateral loads that emulate the modal shape of the respective mode until the roof displacement reaches a prescribed value. The prescribed displacement of each frame for each mode is limited to a drift ratio of 0.02.

The 9-story building was designed for Site Class D, whereas the 3-story, 5-story, and 7-story frames were designed for Site Class C. The higher yield force observed for the first and second modes of the 9-story frame when compared to the other three frames is due to the inherent demand of higher yield force for a higher seismic coefficient. For the first mode pushover case, yielding mostly occurred at lower stories with plastic hinges forming at the column base and beams in the first and second stories, whereas in the second mode case much of the yielding occurred at upper stories, primarily at the level where the lateral force pattern for the second mode shape changes sign.

Following the procedure outlined above, the force–displacement relations for the equivalent SDOF systems that correspond to the first and second modes of the MDOF frames are determined and shown in Figs. 3(a)

Table 1 Periods of vibration and effective modal masses

Frame	3-Story	5-Story	7-Story	9-Story
Period T_1 (s)	1.06	1.48	1.85	2.14
Period T_2 (s)	0.35	0.53	0.66	0.80
M_1^*(10^3 kg)	384.39	639.89	906.24	3719.69
M_2^*(10^3 kg)	48.86	86.51	113.66	484.21
ΣM_r^* (10^3 kg)	433.25	726.39	1019.89	4203.89
System mass m (10^3 kg)	442.53	761.59	1080.83	4504.57
$\Sigma M_r^*/m$	97.9%	95.4%	94.4%	93.3%

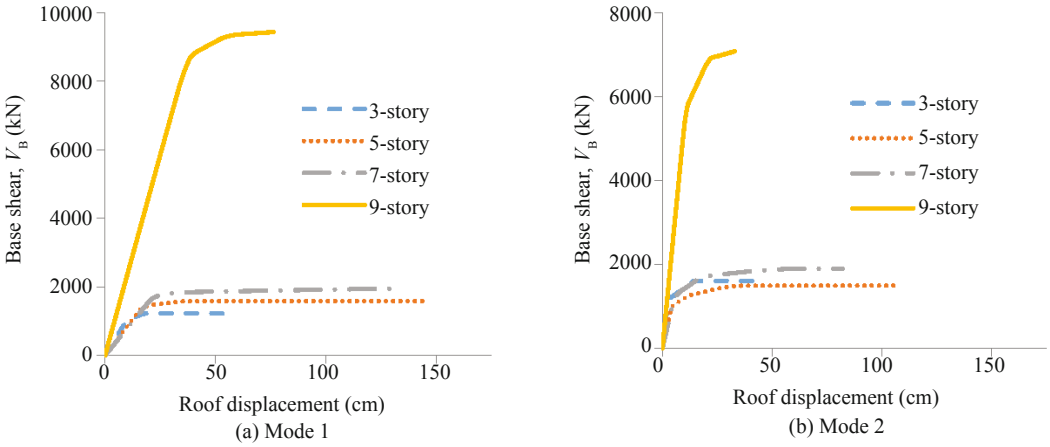

Fig. 2 MDOF system pushover curves

and 3(b). Note that the yield forces for these systems are higher for the second modes indicating that most of the yielding is occurring in the first mode. A summary of the yield forces and other parameters used in the input energy analysis for the equivalent SDOFs is given in Table 2.

To demonstrate the applicability and validity of the proposed procedure, the four MDOF frames and their modal equivalent SDOF systems are subjected to the fault normal and fault parallel components of three earthquake ground motions. The characteristics of these earthquakes are given in Table 3. These earthquakes are scaled in such a way that they will cause yielding in the frames without collapse and/or excessive distress. The scale factors used are summarized in Table 4.

A total of 72 earthquake time history analyses were performed: 48 using BISPEC (2012) for the equivalent SDOF components and 24 using Perform-3D (2011) for the MDOF systems. The input energy for both systems were analyzed and compared. The results are presented in Figs. 4 to 7 for the 3-, 5-, 7- and 9-story frames, respectively, and the ratios of the input energy for the equivalent SDOF systems to that of the MDOF frames (IE_{ESDOF}/IE_{MDOF}) are summarized in Table 5. From this comparison, it can be concluded that Eq. (20a), used in conjunction with the proposed procedure, is capable of producing a reasonable estimate of the input energy for MDOF systems using input energy from their associated equivalent SDOF components.

6 Hysteretic energy distribution

Although Eq. (20b) provides a means to convert the hysteretic energy of a SDOF system for application in a MDOF building structure, a distribution scheme is still needed to distribute this energy to each story of the multistory frame. This is analogous to the use of a distribution scheme to distribute the base shear over the height of a building in a force-based design approach. Using a statistical approach, Seneviratna and Krawinkler (1997) as well as Shen and Akbas (1999) investigated the hysteretic energy (HE) distribution over the height of a building but were not able to identify any consistent pattern. On the other hand, Akbas *et al.* (2001) from their study of regular frames with a damping ratio of ζ = 0.02 concluded that hysteretic energy distribution along the height is linear. Ye *et al.* (2009) counter-argued

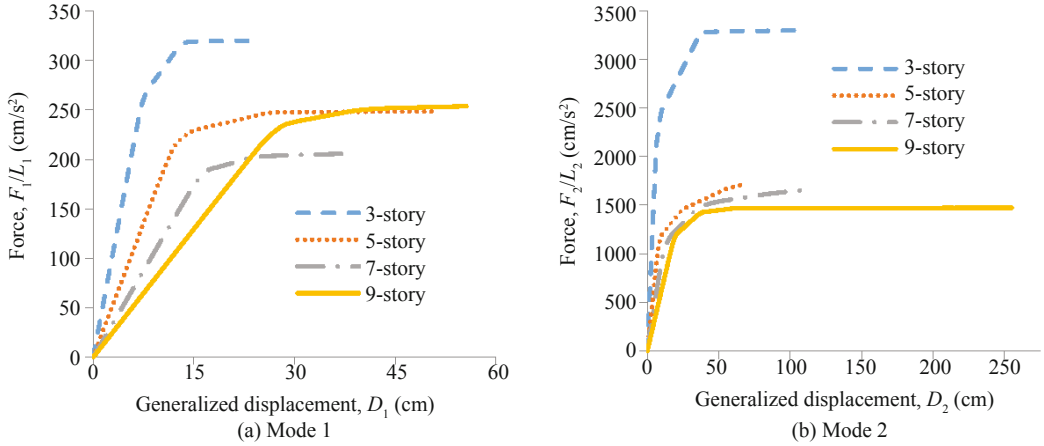

Fig. 3 Equivalent SDOF system force-deformation relationships

Table 2 Equivalent SDOF parameters

Mode 1					
Frame	Period (s)	D_{1y} (cm)	F_{1y}/L_1(cm/s^2)	α	Γ_1
3-Story	1.06	8.2	289.6	0.07	1.481
5-Story	1.49	13.21	236.3	0.03	1.912
7-Story	1.85	17.02	196.4	0.02	5.175
9-Story	2.14	27.94	241.3	0.06	4.609
Mode 2					
Frame	Period (s)	D_{2y} (cm)	F_{2y}/L_2(cm/s^2)	α	Γ_2
3-Story	0.342	8.13	2743.2	0.02	0.528
5-Story	0.537	9.78	1341.2	0.05	0.703
7-Story	0.654	14.61	1346.2	0.035	0.649
9-Story	0.781	21.59	1397	0.01	1.663

Table 3 Ground motions used for the verification study (Units are in centimeters and seconds)

Ground motion	Fault normal (FN) component			Fault parallel (FP) component		
	CAV	PGA	PGV	CAV	PGA	PGV
Loma Prieta	185.12	62.77	14.98	135.46	38.84	6.02
Northridge-01	230.69	64.06	3.16	172.37	35.69	1.99
Chi-Chi Taiwan	310.39	69.55	7.51	273.05	50.7	7.31

Table 4 Ground motion scaling factors

Ground motion	Loma Prieta (LP)		Northridge-01 (NR)		Chi-Chi (CHI)	
Frame	FN	FP	FN	FP	FN	FP
3-Story	7.14	12.5	5	11	7.14	10
5-Story	8.33	12.5	5	11	7.14	10
7-Story	8.33	12.5	5	11	7.14	10
9-Story	6.5	12.5	5	11	7.14	10

Table 5 IE_{ESDOF} /IE_{MDOF} for multi-story frames (FN = Fault normal, FP = Fault parallel)

	Input energy ratio, IE_{ESDOF} /IE_{MDOF}					
Record	LP-FN	LP-FP	NR-FN	NR-FP	CHI-FN	CHI-FP
3-Story	0.98	1.08	1.11	0.98	0.99	0.99
5-Story	0.92	1.12	0.97	0.96	1.03	0.82
7-Story	1.11	0.89	0.94	1.06	0.81	0.84
9-Story	1.03	1.11	0.77	1.00	0.90	0.76

that hysteretic energy distribution could be considered linear only for damping ratio $\zeta > 0.1$ and proposed linear equations to distribute the *HE* over the building height for structures with damping ratio $\zeta > 0.1$. It is imperative to note that such high damping could only be attained if supplementary damping devices are installed in the structure. Based on a multi-mode pushover analysis approach, Chou and Uang (2003) established a relationship between the end rotations and hysteretic energy of the framing elements in a particular story, and recommended distribution patterns, which they referred to as energy shapes, at different stages of loading. These energy shapes are functions of cumulative end rotations in each story. They proposed three different energy shapes for each of the first two modes and distributed the hysteretic energy contribution by each mode to the different stories of the structure. More recently, Wang and Yi (2012) developed a procedure for estimating the total hysteretic energy for MDOF systems from their equivalent SDOF systems and proposed the following

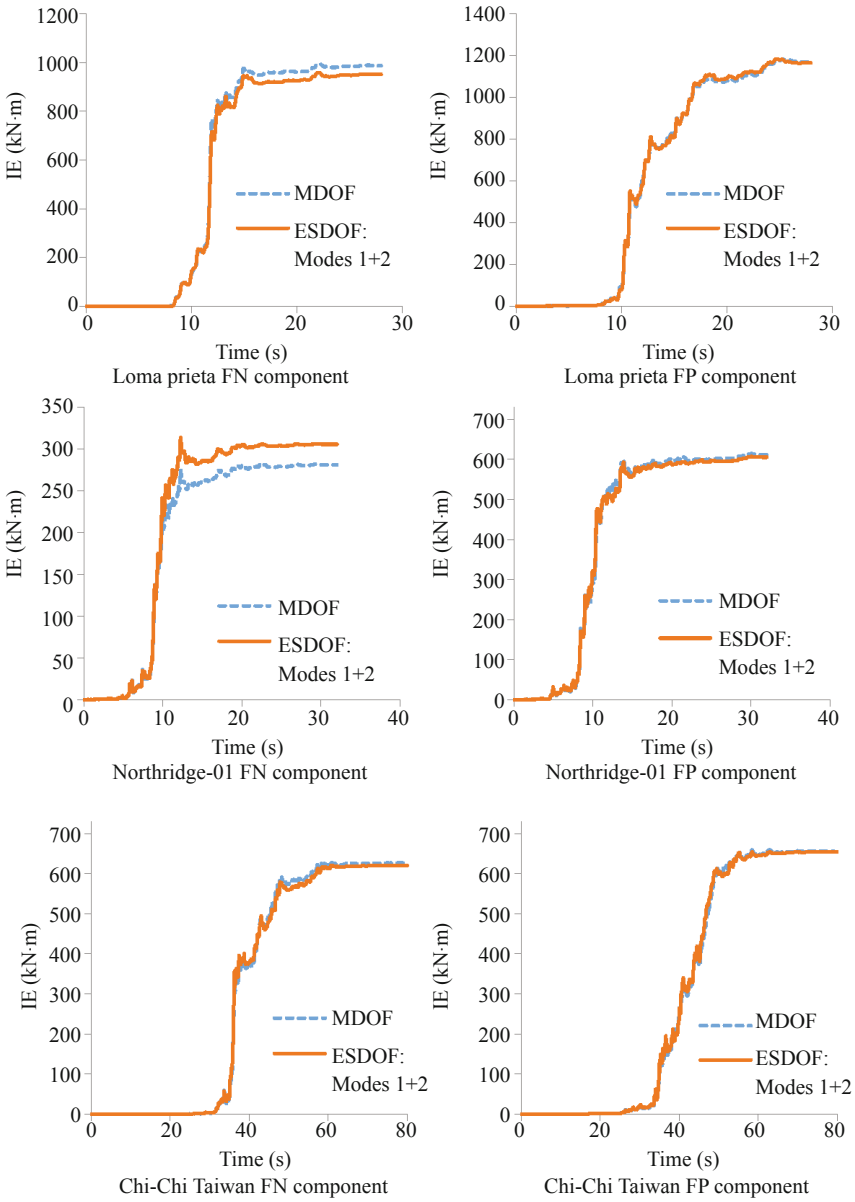

Fig. 4 Input energy (IE) time histories for the three-story frame

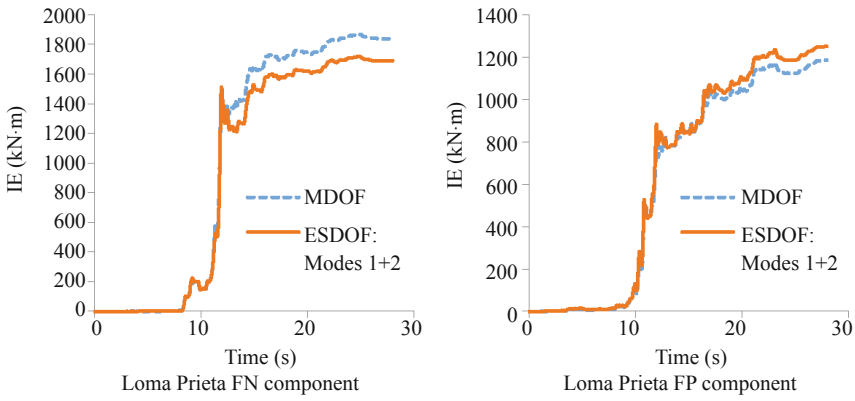

Fig. 5 Input energy (IE) time histories for the five-story frame

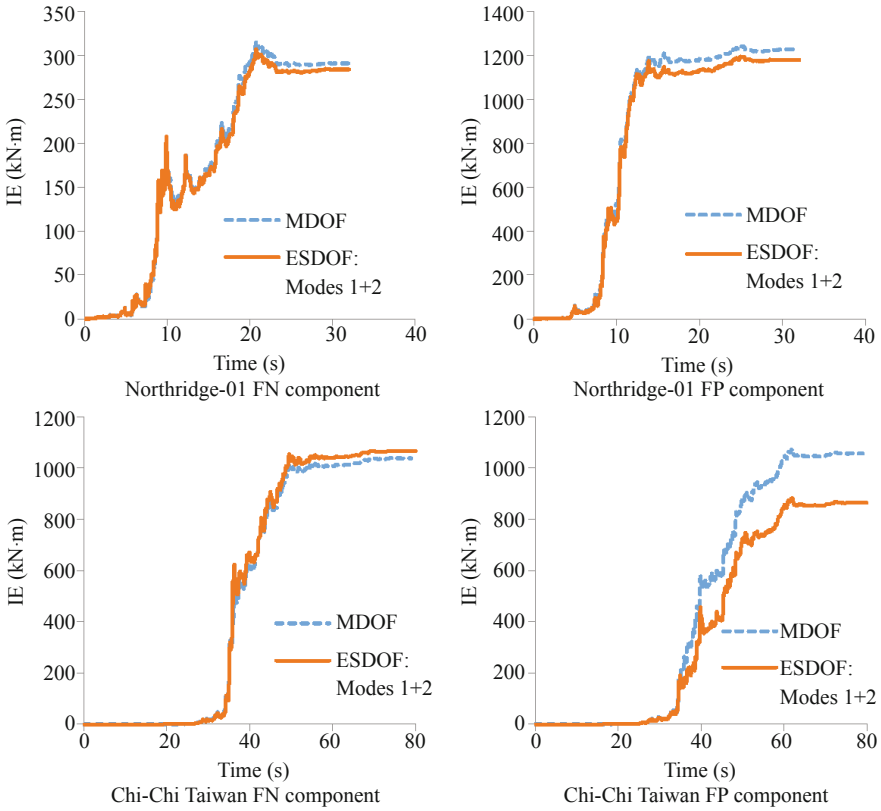

Fig. 5 Continued

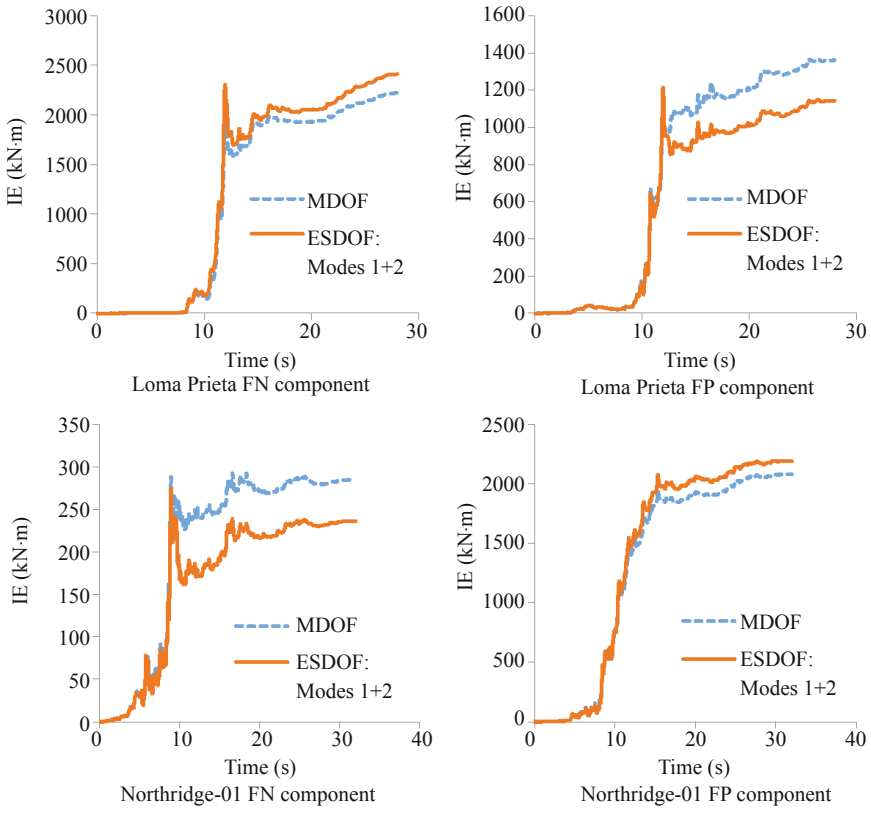

Fig. 6 Input energy (IE) time histories for the seven-story frame

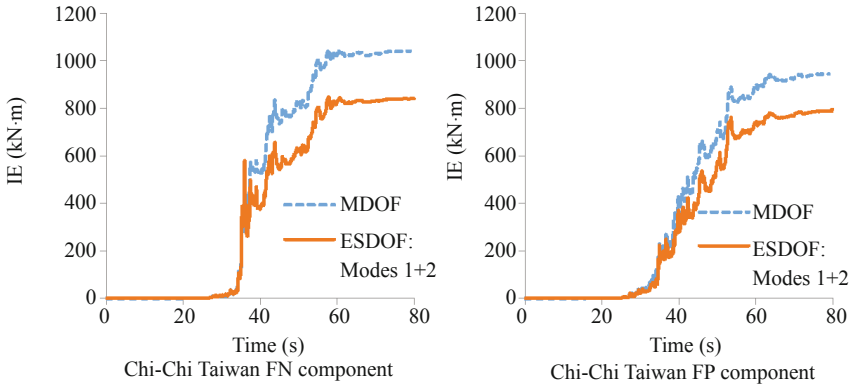

Fig. 6 Continued

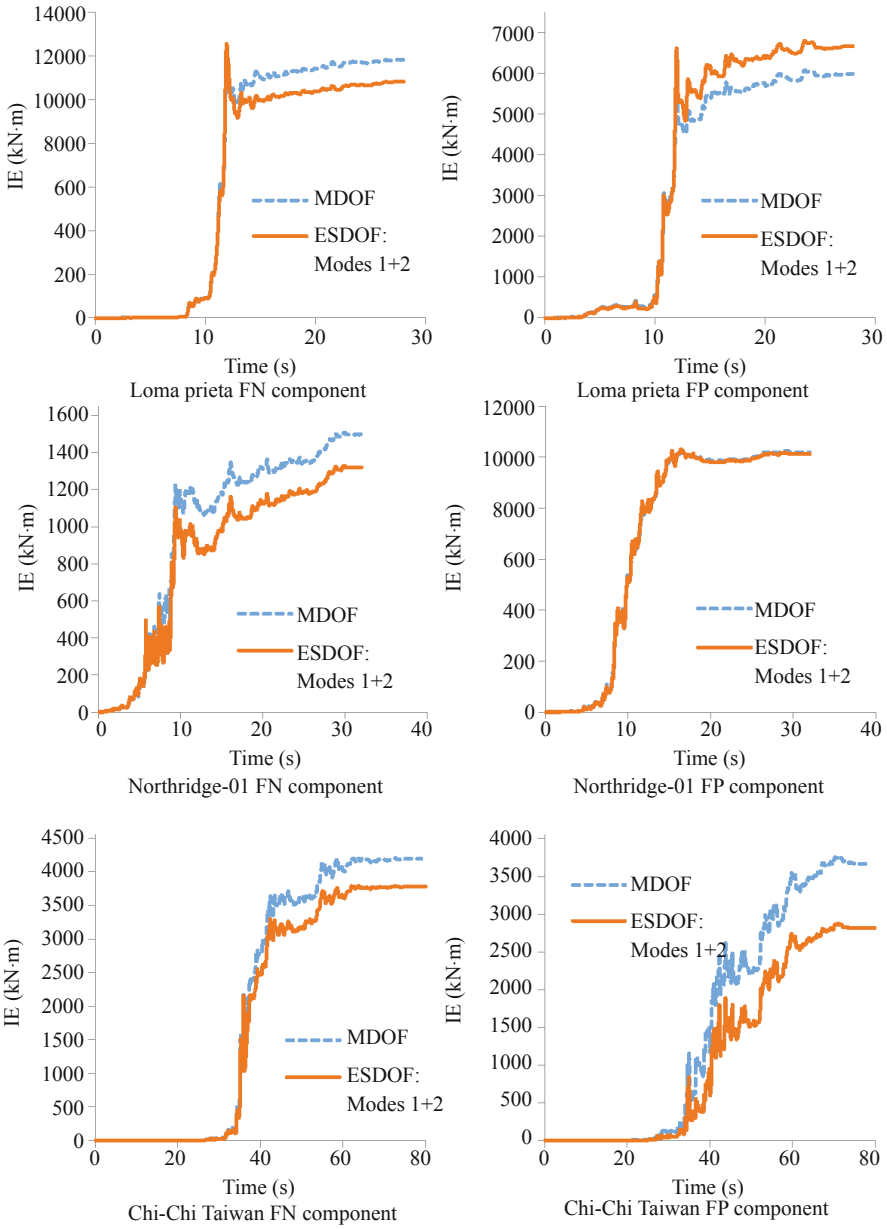

Fig. 7 Input energy (IE) time histories for the nine-story frame

distribution equation of hysteretic energy for MDOF systems.

$$\mathrm{HE}_{i,j} = \frac{(\sum_{k=i}^{N} m_k \phi_{k,j})\Delta\phi_{i,j}}{\sum_{k=1}^{N} m_k \phi_{k,j}^2} \mathrm{HE}_{\mathrm{total},j} \tag{21}$$

where $\phi_{i,j}$ = displacement at story i for mode j; $\Delta\phi_{i,j}$ = $\phi_{i,j}$ - $\phi_{i\text{-}1,j}$; m_k = mass of story k; $\mathrm{HE}_{i,j}$ = hysteretic energy dissipated by story i for mode j; $\mathrm{HE}_{\mathrm{total},j}$ = total hysteretic energy for mode j and N = number of stories. Upon application of the procedure for three six-story pin supported buildings subjected to a total of nine ground motions, three records each on hard, intermediate and soft soils, they concluded that their proposed equation was suitable for hard soil site and for buildings whose lateral displacement shape was controlled by the first mode shape.

For a given mode, it should be noted that Eq. (21) can be expressed in terms of work done by external forces applied at each story level in acting through the story displacements. This is because in modal pushover analysis, it is common practice to define the lateral load pattern as the product of the mass matrix and mode shape vector. Therefore, Eq. (21) can be rewritten as

$$R_i = \frac{\mathrm{HE}_{i,j}}{\mathrm{HE}_{\mathrm{total},j}} \approx \frac{\mathrm{WE}_i}{\mathrm{WE}_{\mathrm{total}}} = \frac{(\sum_{k=i}^{N} F_k)\Delta d_i}{\sum_{k=1}^{N} F_k d_k} \tag{22}$$

where N is the number of stories, R_i is the energy ratio for story i, WE_i and $\mathrm{WE}_{\mathrm{total}}$ are the work done by story i and the total work done by the frame for a given mode, respectively; F_k is the modal force acting at story k, d_k is the displacement at story k, and $\Delta d_i = d_i\text{-}d_{i\text{-}1}$ is the interstory displacement of story i.

An advantage of expressing the energy ratio as a function of work done is that the change in energy distribution due to inelasticity can be more conveniently captured. As shown in Fig. 8, a study by the authors has shown that Eq. (22) performs better than schemes proposed by others when compared to the actual hysteretic distribution but tends to underestimate the hysteretic

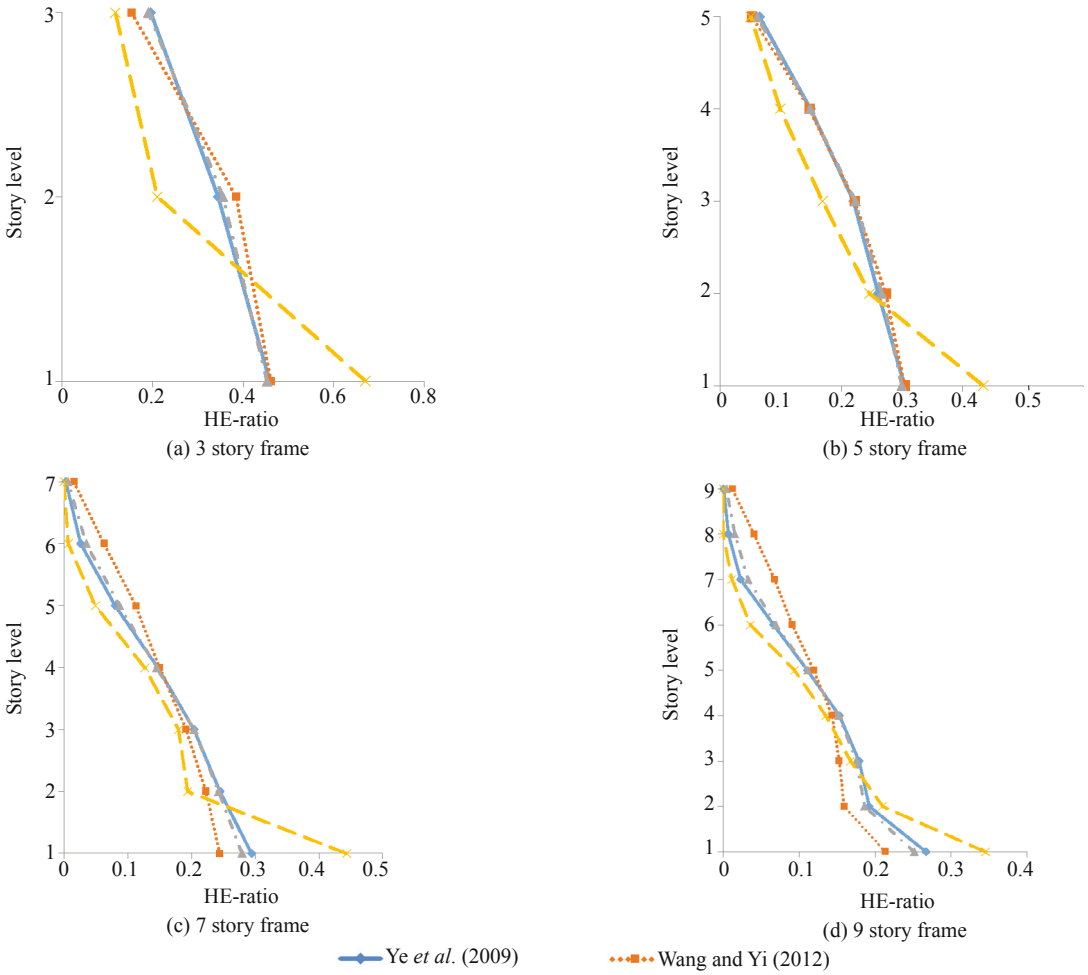

Fig. 8 Comparison of hysteretic energy distribution

energy demand at the lower stories (especially the first story) and overestimate the demand at upper stories. This is because when a multistory frame is pushed beyond the performance limit of life safety, plastic hinges tend to form at the base where the moment, shear and axial force are the highest. To obtain better solutions, it is proposed that Eq. (22) be modified to

$$R_i = \frac{\mathrm{WE}_i}{\mathrm{WE}_{\mathrm{total}}} = \begin{cases} \dfrac{2(\sum_{k=i}^{N} F_k)\Delta d_i}{(\sum_{k=1}^{N} F_k)d_1 + \sum_{k=1}^{N} F_k d_k} & \text{for } i = 1 \\ \dfrac{(\sum_{k=i}^{N} F_k)\Delta d_i}{(\sum_{k=1}^{N} F_k)d_1 + \sum_{k=1}^{N} F_k d_k} & \text{for } i \geq 2 \end{cases} \tag{23}$$

To use the above equation, a designer only needs to compute the modal forces for each mode using any existing procedure, apply these forces to the multistory frame, and calculate the displacements due to these modal forces. For comparison, the hysteretic energy distributions calculated using Eq. (23) were plotted in Fig. 9 along with the actual hysteretic distributions. It can be seen that the proposed distribution equation produces results that match reasonably well with the actual hysteretic energy distributions for the 3-, 5-, 7- and 9-story frames.

7 Energy-based seismic design

The objective of energy-based seismic design (EBSD) is to design a structure so its energy dissipation capacity exceeds the hysteretic energy demand from a design earthquake or a set of design earthquakes, i.e.,

$$(\text{Hysteretic energy})_{\text{capacity}} \geq (\text{Hysteretic energy})_{\text{demand}} \tag{24}$$

For a structure subject to a given earthquake, the right side of Eq. (24) can be evaluated using a hysteretic energy spectrum in conjunction with Eqs. (20b) and (23). To evaluate the left side of the equation, information on the type of frame and energy dissipative devices used (Foti, *et al.*, 1998; Benavent-Climent, 2011; Liang, *et al*., 2012) are needed. In the present study, moment

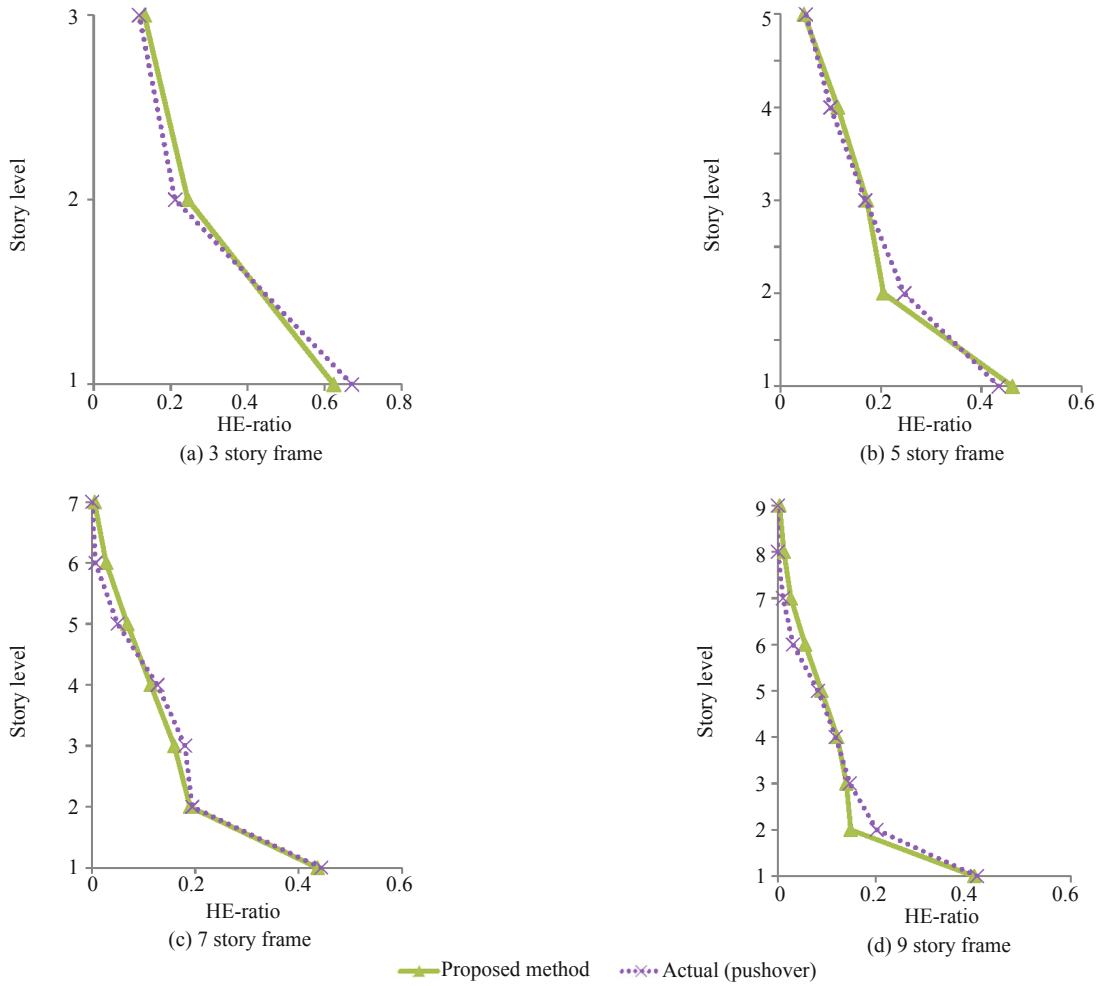

Fig. 9 Performance of proposed hysteretic energy distribution

resisting steel frames are used and it is assumed that no supplementary energy dissipative devices are present. As a result, EBSD in essence is a plastic design and the formation of plastic hinges, and the amount of rotation they experience constitute the energy dissipative capacity of the structure.

7.1 Energy-based seismic design and plastic design relations

The underlining concept of plastic design of steel structures lies in the formation of plastic hinges and the resulting collapse mechanisms. Consider a portal frame shown in Fig. 10 subject to a horizontal joint load H and a concentrated span load P. The work equations for the two independent collapse mechanisms shown using the geometry of the structure (h, b), plastic moment capacities of the beam and columns (M_{pb}, M_{pc}), the applied forces (H, P) and the anticipated plastic rotations at collapse (θ_p) can be written as:

$$\begin{aligned} &\text{External work} = \text{Internal work} \\ &\text{Sway mechanism} \quad H\times(h\times\theta_p) = (2M_{pc}+2M_{pb})\times\theta_p \\ &\text{Beam mechanism} \quad P\times(\frac{b}{2}\times\theta_p) = (4M_{pb})\times\theta_p \end{aligned} \tag{25}$$

For design purpose, the external and internal work can be conceived as the energy demand and dissipation capacity, respectively. Henceforth, for energy-based seismic design the external work can be replaced by hysteretic energy demand. This approach has been used by Estes and Anderson (2004) in an energy-based seismic design of steel frames and Terapathana (2012) for an energy-based seismic design of reinforced concrete structures. As for the energy dissipation, it should be noted that the right hand side of Eq. (25) does not involve load reversal and is monotonic. Thus, it is necessary to adjust the static monotonic hysteretic energy given by the right hand side of Eq. (25) in order to correlate it to the dynamic hysteretic energy capacity of structures subjected to earthquake loads.

For seismic evaluation of existing reinforced concrete structures, ATC 40 (1996) has suggested the use of a dynamic to monotonic hysteretic energy ratio of four, subject to reduction factors to account for a reduction in the dynamic hysteretic energy due to pinching nature of the hysteresis behavior of concrete sections. For moment resisting steel frames, with properly designed connections and stable hysteresis, it is reasonable to consider a factor of four as the ratio of dynamic-to-monotonic hysteretic energy. The justification behind the use of a factor of four can be explained from the energy calculation of one cycle of an idealized hysteresis loop as shown in Fig. 11, where it can be seen that with stable hysteresis behavior devoid of any stiffness or strength degradation, the full cyclic area is four times the monotonic area. A dynamic-to-static hysteretic ratio of four will be used in this study to design an earthquake resistant moment resisting steel frames based on energy method. For instance, for the frame mechanism shown in Fig. 10(a), the hysteretic energy capacity given by the left hand side of Eq. (24) shall be greater than or equal to the hysteretic energy demand due to a design earthquake, i.e.,

$$4.0\times[(2M_{pc}+2M_{pb})\times\theta_p]\geq(\text{HE})_{\text{demand}} \tag{26}$$

where $(\text{HE})_{\text{demand}}$ = the hysteretic energy demand due to the design earthquake or suite of earthquakes.

To a practicing engineer, the effect of earthquake on structures is more readily understandable when it is tied to the resulting horizontal motions/deformations of the structure. This is a useful observation to assess the applicability of Eq. (25) to the different possible collapse mechanisms a structure may undergo. For the beam mechanism shown Fig. 10(b), it is obvious that the mechanism is related to vertical loads and is minimally affected by earthquake events. Thus, equating

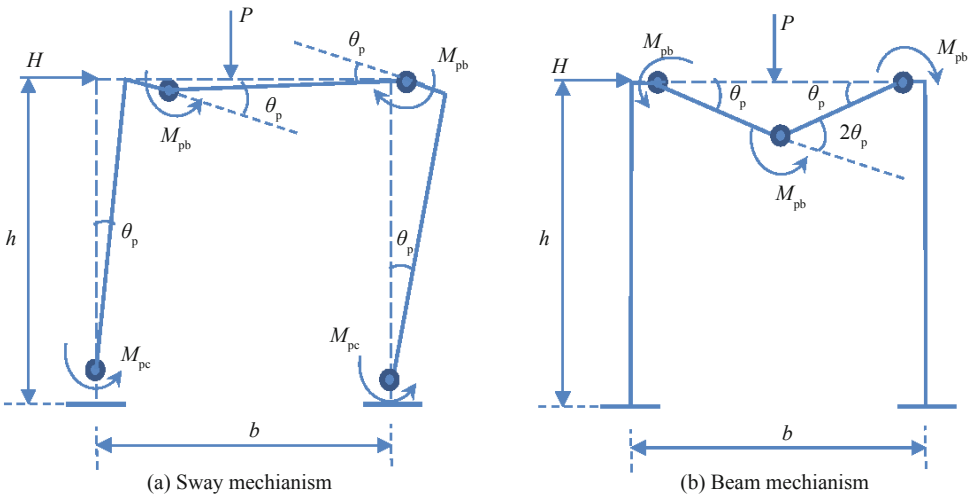

Fig. 10 Collapse mechanisms of a portal frame ($M_{pb} < M_{pc}$)

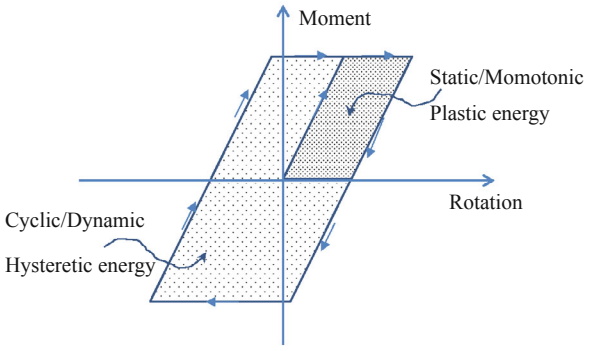

Fig. 11 Elastic-plastic hysteresis loop

the external work causing a beam mechanism to a hysteretic energy demand due to an earthquake renders it unrealistic. Similarly, for a combined mechanism of sway and beam mechanisms, vertical loads are involved and the resulting external work cannot be fully related to the hysteretic energy demand due to an earthquake. As a result, the beam and combined collapse mechanisms will be discarded in the energy-based seismic design formulation in this study without significantly affecting the final design result. This argument is supported by Estes and Anderson (2004) who showed that vertical load mechanisms are not significant when earthquake forces are considered.

In order to optimize the design of the beam and columns (i.e., obtaining the best possible combination of M_{pb} and M_{pc}), the plastic hinge rotation θ_p in Eq. (26) needs to be determined. Per FEMA 350 (2000), moment resisting steel frames are capable of developing large plastic rotations, in the order of 0.02 radian or larger, without significant strength degradation, and according to FEMA 267A (1997) Interim Advisory No.1, based on the work of SAC and other researchers on full-scale tests done after the Northridge earthquake, a plastic rotation of 0.025 to 0.030 was recommended for steel moment connections. Thus, in this study a design plastic rotation of 0.03 radians is used.

A design method is deemed appropriate if it ensures that the resulting structure is safe against the design actions and is also cost effective. The cost of a structure is affected by a number of factors and for simplicity, member size is used in this study as an indicator of cost. Since member size and member weight are often related, the cost aspect of a design can be addressed by minimizing the weight of the structure. For moment resisting frames, the weight of beams and columns in most cases can be reasonably associated with their corresponding plastic moment capacity. Thus, a weight function can be expressed in terms of the length of the members and their plastic moment capacities. For instance, for the frame in Fig. 10, the weight function can be written as

$$W = 2 \times h \times M_{pc} + b \times M_{pb} \tag{27}$$

The use of this weight function as a design parameter reduces the energy-based seismic design to an optimization problem. For energy-based seismic design, the objective function is the weight function whereas the inequalities of the collapse mechanisms form the constraint equations. In moment resisting frame design, additional constraints such as beam to column capacity ratio, that arise from code or detailing requirements may need to be considered. For instance, for the frame in Fig. 10, the mathematical formulation of the minimization problem can be written as:

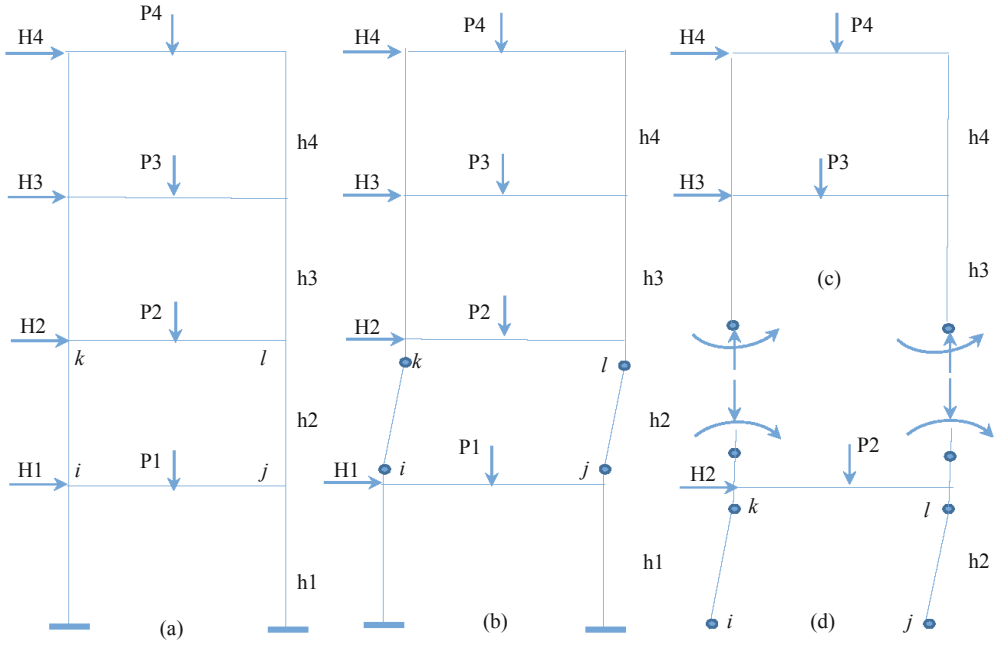

Fig. 12 Story and frame collapse mechanisms

Objective function:

Minimize the weight function: $W = 2 \times h \times M_{pc} + b \times M_{pb}$

Subject to the constraint equations:

$4.0 \times [(2M_{pc} + 2M_{pb}) \times \theta_p] \geq (\text{HE})_{demand}$; Strong Column – Weak Beam scenario

$4.0 \times [4M_{pc} \times \theta_p] \geq (\text{HE})_{demand}$; Strong Beam – Weak Column scenario

$M_{pc} - M_{pb} \geq 1.0$; Code requirement

where M_{pb}, $M_{pc} > 0$. (Note that if there is more than one column and one beam meeting at a joint, the last constraint equation should be expressed as $\Sigma M_{pc} - \Sigma M_{pb} \geq 1.0$)

The above minimization for M_{pc} and M_{pb} can be easily achieved by using a Microsoft Excel built-in analysis function called the Simplex Method, which is a method for solving problems in linear programming.

7.2 Application to multistory frames

While the formulation of an optimization problem for an energy-based seismic design of a single story portal frame is relatively simple, the formulation for multistory frames can conceivably involve many possible collapse mechanisms with many feasible constraint equations and could become rather complex. Ridha and Wright (1967) proposed a classical safe approach called a story-wise optimization that reduces the plastic design of multistory frames into the design of a series of single story frames stacked vertically. In this approach, the design is accomplished on a story-to-story basis, starting with the topmost story and moving down one story at a time. The story-wise approach was also used by Disque (1971) for the design of multistory braced frames and was adopted by Estes and Anderson (2004) and Terapathana (2012).

To illustrate the concept, consider a four-story frame shown in Fig. 12(a) with possible sway mechanisms developed in each story. According to Ridha and Wright (1967), the design of the frame for safety against the sway mechanism occurring in the second story of the entire frame as shown in Fig. 12(b) can be achieved by simultaneously satisfying the design requirements for the standalone story mechanism shown in Fig. 12(d) and the resulting mechanism of the story above it as shown in Fig. 12(c). This can be easily verified by comparing the external and internal work equations of the collapse mechanisms shown in Figs. 12(b)–12(d).

Because the plastic capacity of compressive members is affected by the simultaneous action of axial force and bending moment, especially in multistory frames where gravity loads increase toward the lower stories, it is necessary to include the effect of axial force in the formulation of the energy-based seismic design. One way to incorporate axial force effect into EBSD is to use code recommended axial force-bending moment interaction equations such as the ones given in the ANSI/AISC 360-10 (2010). That is,

$$\begin{aligned} &\frac{P_r}{P_c} + \frac{8}{9}\left(\frac{M_{rx}}{M_{cx}} + \frac{M_{ry}}{M_{cy}}\right) \leq 1.0 \quad \text{for } \frac{P_r}{P_c} \geq 0.2 \\ &\frac{P_r}{2P_c} + \left(\frac{M_{rx}}{M_{cx}} + \frac{M_{ry}}{M_{cy}}\right) \leq 1.0 \quad \text{for } \frac{P_r}{P_c} < 0.2 \end{aligned} \tag{28}$$

where the subscripts c, r, x, and y represent the design strength, required strength, strong axis and weak axis bending, respectively. For uniaxial bending about the strong axis, which is often the case for frame analysis and design, the subscripts x and y can be dropped from the equations and after rearranging, the interaction equations take the form

$$\begin{aligned} &M_c \geq \frac{8}{9}\left(\frac{1}{(1-\frac{P_r}{P_c})}\right) M_r = \beta_m M_r \quad \text{for } \frac{P_r}{P_c} \geq 0.2 \\ &M_c \geq \left(\frac{1}{(1-\frac{P_r}{2P_c})}\right) M_r = \beta_m M_r \quad \text{for } \frac{P_r}{P_c} < 0.2 \end{aligned} \tag{29}$$

The modification factor β_m accounts for the reduction in the design moment capacity M_c due to the presence of an axial force by applying an amplification factor to the required moment capacity M_r obtained per the energy-based seismic design procedure. According to ANSI/AISC 360-10 (2010) Load and Resistance Factor Design (LFRD) method, the design axial force (P_c) and the design moment (M_c) capacities of a member are given by $\varphi_c P_n$ and $\varphi_b M_n$, respectively, where φ_c and φ_b are resistance factors for compression and bending, respectively. Because these factors are likely to be different for different specifications and they change with time, they are both taken as unity in the following design examples. The primary objective here is to demonstrate how the energy-based design process can be applied without regard to the exact values of resistance factors used. ANSI/AISC 360-10 (2010) also provides equations for determining the nominal capacities P_n and M_n for almost all commonly used structural shapes. However, for purpose of demonstrating the proposed EBSD procedure, all members are assumed compact and adequately braced against lateral torsional instability; thus, the nominal capacities for flexure and compression are calculated as follows.

$$M_n = F_y Z \quad \text{and} \quad P_n = F_{cr} A_g \tag{30}$$

where F_y = yield stress, Z = plastic section modulus about the axis of bending, F_{cr} = axial stress capacity assuming stable hysteresis behavior devoid of any stiffness or strength degradation, and A_g = gross cross-sectional area of the member.

8 Proposed energy-based seismic design procedure

The procedure for applying the proposed EBSD is given as follows:

(1) Perform preliminary member design.

(2) Determine modal properties of the frame.

(3) Calculate the normalized input energy per unit mass.

(4) Obtain the hysteretic energy per unit mass.

(5) Determine the MDOF hysteretic energy demand and its distribution over the frame height.

(6) Optimize the member sizes using the Simplex method.

(7) Account for the effect of axial force on the plastic moment capacity.

(8) Compare the energy capacity with the associated demand and make sure capacity exceeds demand.

(9) Repeat the above steps until convergence.

Convergence is said to have been achieved when member sizes from two consecutive iterations do not change appreciably. The above procedure for carrying out an EBSD for multistory moment resisting frames is summarized in the form of a flowchart shown in Fig. 13. The details involved in each step will be demonstrated in the following section through a design example of a three-story frame. The procedure outlined above and flowchart shown in Fig. 13 is simple and easy to follow but the design, like any other designs, needs some engineering judgment in its execution.

9 Example design

The three-story frame shown in Fig. 14 is to be designed using the above proposed EBSD procedure. It is a moment resisting steel frame consists of beams and columns with rigid connections. The roof level beams are subjected to uniform dead and live loads of 36.5 kN/m and 25.5 kN/m, respectively, while the dead and live loads on the remaining floor beams are 43.8 kN/m and 32.8 kN/m, respectively. The system or seismic mass m is consisted of 100% of the dead loads and 25% the live loads plus self-weight of the frame. To incorporate diaphragm action, diaphragm constraints are employed to force the joints at a given floor to displace the same horizontally.

The frame is assumed to be built in a location with site soil Class C. A set of five earthquakes from the PEER Beta Data Base are used and scaled to match an IBC (2012) response spectrum. The response spectrum is generated using a built-in procedure in SAP 2000 for soil Class C at a site with zip code 94704. The location is chosen because it lies in one of the highly seismic active areas in the west coast of the United States. The design earthquakes are selected to be the Horizontal-1 (the

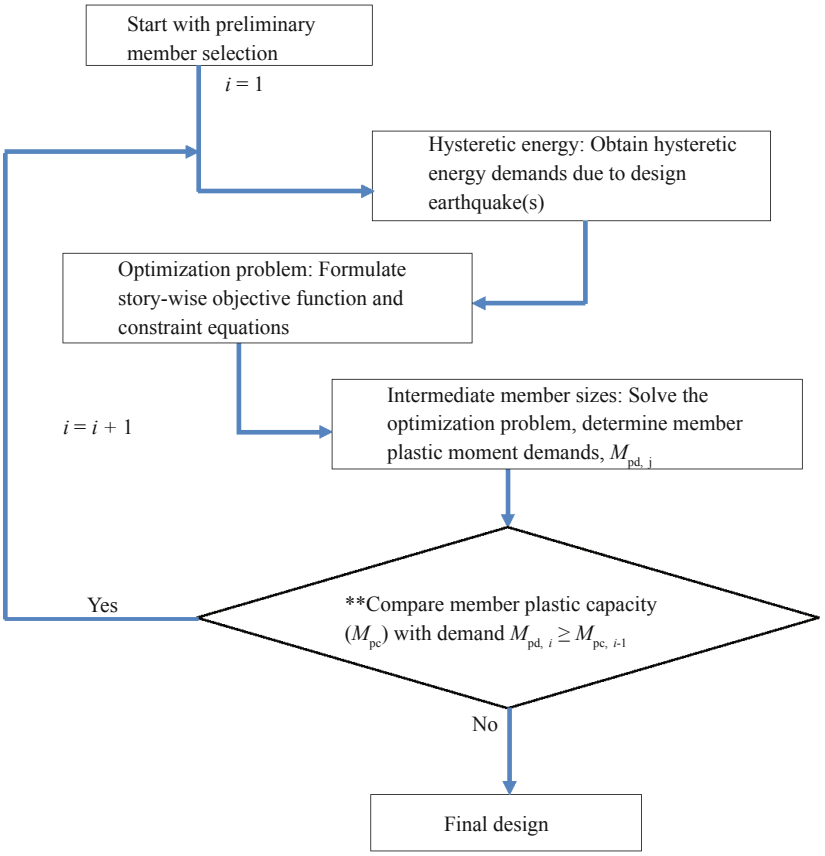

**It is also required to check that $M_{pc,\ i\text{-}1}$ is not excessively greater than $M_{pd,\ i}$

Fig. 13 Flowchart: energy based seismic design

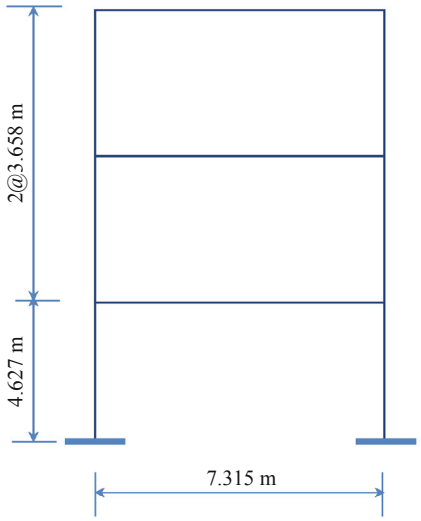

Fig. 14 Design example: three story - one bay frame

main horizontal direction) component of the respective earthquake records. Details of the selected earthquakes are given in Table 6.

Step 1: Preliminary member sizes

The preliminary members of the frame are determined from a gravity load design exercise using the ANSI/AISC 360-10 LFRD procedure within the SAP 2000 (2014) structural analysis and design software. The results are presented below.

Preliminary column sizes		Preliminary beam sizes	
Story	Size	Floor level	Size
1st	W14 × 90	1st	W18 × 76
2nd	W14 × 90	2nd	W18 × 76
3rd	W14 × 90	Roof	W18 × 76

Step 2: Modal properties

Using these preliminary member sizes, modal properties for the first two modes that constitute more than 90% of the seismic mass are calculated and the results are given below.

	Period (s)	M^*_r, (kg)	M^*_r (m)	Ductility, (μ)
Mode 1	0.83	106×10^3	0.889	4
Mode 2	0.25	114×10^3	0.095	4
		ΣM^*_r(m) =	98.4%	

Step 3: Normalized input energy per unit mass (NE)

The normalized input energy spectra for an equivalent SDOF for soil Site Class C and hysteretic model BP, the mean+σ *NE* spectra for a design ductility level μ = 4 are calculated using the equations derived in a study by Mezgebo and Lui (2016) given below.

$$a = -0.0507\mu + 1.515 = -0.0507\times4 - 1.515 = 1.312$$

$$b = 0.0137\mu - 0.0569 = 0.0137\times4 - 0.0569 = -0.0021$$

$$T_1 = 0.374\mu^{-0.116} = 0.374\times4^{-0.116} = 0.318\,\text{s}$$

$$C = 0.0069\mu^2 - 0.0657\mu + 0.563 = 0.0069\times4^2 - 0.0657\times4 + 0.563 = 0.411$$

$$T_2 = -0.102\mu + 1.978 = -0.102\times4 - 1.978 = 1.57\,\text{s}$$

$$k = 0.0089\mu^2 - 0.129\mu + 0.946 = 0.0089\times4^2 - 0.129\times4 = 0.572$$

$$n = 0.0072\mu^2 - 0.0124\mu - 0.786 = 0.0072\times4^2 - 0.0124\times4 - 0.786 = -0.702$$

Thus, according to Mezgebo and Lui (2016),

For Mode 1: (T_1 = 0.318 s) < (T = 0.83 s) < (T_2 = 1.57 s)

==> NE = C = 0.41

For Mode 2: (T = 0.25 s) < (T_1 = 0.318 s)

==> NE = $aT + b$ = 1.312×0.25-0.0021 = 0.326

Because NE is defined as the square root of the input energy per unit mass (IE/*m*) divided by the velocity index, VI (= CAV × PGV). Therefore, the input energy per unit mass is given by

$$\text{IE}/m = \text{NE}^2\times\text{CAV}\times\text{PGV}$$

where CAV = Absolute Cumulative Velocity; PGV = Peak Ground Velocity of the design earthquake. Since the frame is to be designed for the mean+σ of the selected design earthquakes, the corresponding mean+σ VI needs to be calculated. The calculation of the mean+σ VI is shown in the table below.

Table 6 Selected design earthquakes (Units are in centimeters and seconds)

Earthquake	Station	Year	CAV	PGA	PGV	Scale
Loma Prieta	Bear Valley #5	1989	291.7	66.81	9.25	11.5
Loma Prieta	Fremont - Mission San Jose	1989	533.84	124.21	14.1	7.5
Loma Prieta	Hayward City Hall - North	1989	205.14	47.96	5.62	18.5
Loma Prieta	SF - Telegraph Hill	1989	114.2	35.01	3.61	25.5
Loma Prieta	Yerba Buena Island	1989	125.58	28.86	4.35	28
Landers	Amboy	1992	921.8	112.86	18.22	6

	(a)	(b)	(c)	(d) = (a × b × c²)
Earthquake	CAV (m/s)	PGV (m/s)	Scale factor	VI (m²/s²)
Loma Prieta	2.916	0.092	11.5	35.654
Loma Prieta	5.339	0.141	7.5	42.337
Loma Prieta	2.051	0.056	18.5	39.409
Loma Prieta	1.142	0.036	25.5	26.783
Loma Prieta	1.256	0.043	28	42.762
Landers	9.218	0.182	6	60.435
			mean + σ VI =	52.325

The input energy per unit mass (IE/*m*) for each mode is now obtained as follows:

Mode 1: IE/*m* = NE²×VI = (0.41)²×52.325 m²/s² = 8.796 m²/s²

Mode 2: IE/*m* = NE²×VI = (0.326)²×52.325 m²/s² = 5.561 m²/s²

Step 4: Hysteretic energy per unit mass (HE/m)

The hysteretic energy per unit mass is calculated from the hysteretic-to-input energy relationships developed in study by Mezgebo and Lui (2016). For soil site Class C, hysteretic model BP, and μ = 4, the mean+σ HE/IE spectral shape constants are given as:

C' = 0.651; T_2 = 2.674 s; a_1' = -0.0247 and b_1' = 0.717

Since the periods of vibrations for Mode 1 and Mode 2 are less than T_2, the HE/IE ratio for both modes is within the constant region of the spectra and is equal to C' = 0.651. The modal hysteretic energies per unit mass are then given by:

Mode 1: HE/*m* = (IE/*m*) × (HE/IE) = 8.796 m²/s²× 0.651 = 5.726 m²/s²

Mode 2: HE/*m* = (IE/*m*) × (HE/IE) = 5.561 m²/s²× 0.651 = 3.62 m²/s²

Step 5: MDOF system total hysteretic energy demand and its distribution

The hysteretic energy demand for MDOF systems can be obtained using the hysteretic energy relationships between MDOF systems and their equivalent SDOF systems presented earlier. Using Eq. (20b), the hysteretic energy demand for the frame is calculated as:

$\text{HE}_{\text{total}} = (M^*_r \times \text{HE}/m)_{\text{Mode 1}} + (M^*_r \times \text{HE}/m)_{\text{Mode 2}}$

HE_{total} = (106×10³ kg) (5.726 m²/s²) + (114×10³ kg) (3.62 m²/s²)

= 650 kN·m

The total hysteretic energy demand should now be distributed to the different levels of the frame according to the hysteretic energy distribution presented in Eq. (23). The forces and displacements to be used in Eq. (23) are obtained from modal pushover analysis results for Mode 1. The design ductility level 4 roughly corresponds to a roof drift ratio of 0.04, which is larger than the conventional value of 0.02 often used for the design of building frames for lateral loads. However, a properly designed frame per current codes rarely passes its elastic limit at a roof drift ratio of 0.02, in which case the use of the energy-based seismic design becomes irrelevant. Therefore, for better distribution of the hysteretic energy demand to the different levels of the structure, the frame is pushed to roof drift ratio of 0.04. The results of the pushover analysis are presented below.

Story	Force (kN)	Displacement (cm)	Story drift (cm)
1	165	22.89	22.89
2	320	39.98	17.09
3	343	46.33	6.35

The total and story level external work done during the pushover are computed as follows.

$$\text{For story 1}: \quad \text{WE}_1 = 2(\sum_{k=1}^{n} F_k)\Delta d_1 = 2 \times (165 + 320 + 343) \times 0.2298 = 379\,\text{kN}\cdot\text{m}$$

$$\text{For story 2}: \quad \text{WE}_2 = (\sum_{k=2}^{n} F_k)\Delta d_2 = (320 + 340) \times 0.1709 = 113\,\text{kN}\cdot\text{m}$$

$$\text{For story 3}: \quad \text{WE}_3 = (\sum_{k=3}^{n} F_k)\Delta d_3 = 343 \times 0.0635 = 22\ \text{kN}\cdot\text{m}$$

$$\text{WE}_{\text{total}} = (\sum_{i=1}^{n} F_i)d_1 + \sum_{i=1}^{n} F_i d_i = (165 + 320 + 343) \times 0.2298 + (165 \times 0.2298) + (320 \times 0.3998) + (343 \times 0.4623) = 514\,\text{kN}\cdot\text{m}$$

The hysteretic energy demands at different story levels are then given as

$$\text{Story 1}: \quad R = \frac{\text{HE}_1}{\text{HE}_{\text{total}}} = \frac{\text{WE}_1}{\text{WE}_{\text{total}}} = \frac{379}{514} = 0.737 \Rightarrow$$

$$\text{HE}_1 = 0.737 \times 650\,\text{kN}\cdot\text{m} = 479\ \text{kN}\cdot\text{m}$$

$$\text{Story 2}: \quad R = \frac{\text{HE}_2}{\text{HE}_{\text{total}}} = \frac{\text{WE}_1}{\text{WE}_{\text{total}}} = \frac{113}{514} = 0.221 \Rightarrow$$

$$\text{HE}_2 = 0.221 \times 650\,\text{kN}\cdot\text{m} = 144\,\text{kN}\cdot\text{m}$$

$$\text{Story 3}: \quad R = \frac{\text{HE}_3}{\text{HE}_{\text{total}}} = \frac{\text{WE}_1}{\text{WE}_{\text{total}}} = \frac{22}{514} = 0.042 \Rightarrow$$

$$\text{HE}_3 = 0.042 \times 650\,\text{kN}\cdot\text{m} = 27.5\,\text{kN}\cdot\text{m}$$

Step 6: Member size optimization

The story-wise optimization of members involves formulating a series of story-wise collapse mechanisms and solving an optimization problem. The optimization problem relates the story level hysteretic energy demand to the collapse mechanism based on internal work done (treated in this study as plastic energy capacity or energy

dissipating capacity). The steps involved in the EBSD method of optimization of member sizes are presented below starting with the third (i.e., top) story. Columns in the same story are assumed to have the same size and the member designation used are: M_{kC} = column member in story k, M_{kB} = beam member in story k.

Optimization of Members in the Third Story

Constraint equation based on mechanism in Fig. 15(a) – Strong beam and weak column

$$4 \times (M_{3C} + M_{3C} + M_{3C} + M_{3C}) \times 0.03 \geq 27.5 \text{ kN·m}$$

Constraint equation based on mechanism in Fig. 15(b) – Strong column and weak beam

$$4 \times (M_{3C} + M_{3C} + M_{3B} + M_{3B}) \times 0.03 \geq 27.5 \text{ kN·m}$$

Additional constraint equation at joints – code requirement

$$M_{3C} - M_{3B} \geq 0$$

and to ensure that the beam and column sizes do not differ significantly and that more realistic values of M_{3C} and M_{3B} are obtained, the following constraint equation that requires that the plastic moment capacity of the beam be at least equal to 60% (an arbitrary value specified by the designer) of the moment capacity of the column is also added.

$$M_{3B} \geq 0.60 M_{3C}$$

Objective Function – Weight, W

$$W = 2\,(3.658\,M_{3C}) + 7.315\,M_{3B}$$

Mathematical formulation of the minimization problem

Minimize:

$$W = 7.315\,M_{3C} + 7.315\,M_{3B}$$

Subject to:

$$0.48\,M_{3C} \geq 27.5 \text{ kN·m}$$

$$0.24\,M_{3C} + 0.24\,M_{3B} \geq 27.5 \text{ kN·m}$$

$$M_{3C} - M_{3B} \geq 0$$

$$M_{3C} \geq 0.60\,M_{3B}$$

where $M_{3B} > 0$, $M_{3C} > 0$

The optimized solution obtained using the Simplex linear solver built in Microsoft Excel is;

$$M_{3C} = 57.4 \text{ kN·m} \text{ and } M_{3B} = 57.4 \text{ kN·m}$$

Optimization of members in the second story

Constraint equation based on mechanism in Fig. 15(c) – Strong beam and weak column

$$4 \times (M_{2C} + M_{2C} + M_{2C} + M_{2C}) \times 0.03 - 4 \times (57.4+57.4) \times$$

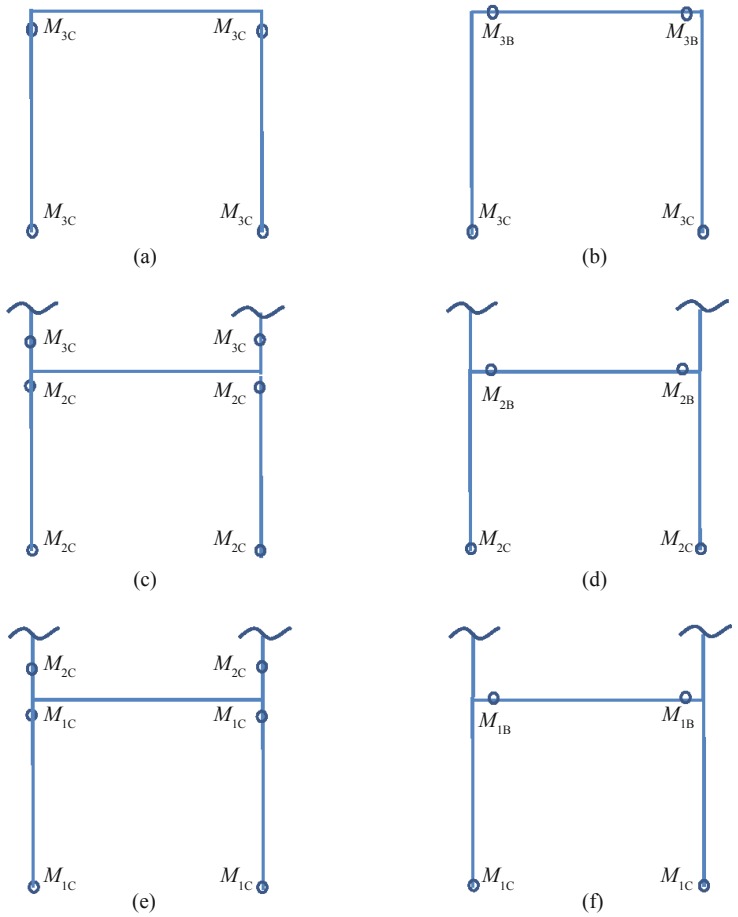

Fig. 15 Story-based mechanisms

$0.03 \geq 144$ kN·m

Constraint equation based on mechanism in Fig. 15(d) – Strong column and weak beam

$$4 \times (M_{2C} + M_{2C} + M_{2B} + M_{2B}) \times 0.03 \geq 144 \text{ kN·m}$$

Additional constraint equation at joints – code requirement

$$M_{2C} + 57.24 - M_{2B} \geq 0$$

Objective Function – Weight, W

$$W = 3.658\, M_{2C} + 3.658\, M_{2C} + 7.315\, M_{2B}$$

Mathematical formulation of the minimization problem

Minimize:

$$W = 7.315\, M_{2C} + 7.315\, M_{2B}$$

Subject to:

$$0.48\, M_{2C} \geq 157 \text{ kN·m}$$

$$0.24\, M_{2C} + 0.24\, M_{2B} \geq 144 \text{ kN·m}$$

$$M_{2C} - M_{2B} \geq 0$$

$$M_{2B} \geq 0.60\, M_{2C}$$

where $M_{2B} > 0,\ M_{2C} > 0$

The optimized solution obtained using the Simplex linear solver built in Microsoft Excel is

$$M_{2C} = 373 \text{ kN·m and } M_{2B} = 224 \text{ kN·m}$$

Optimization of members in the first story

Constraint equation based on mechanism in Fig. 15(e) – Strong beam and weak column

$$4 \times (M_{1C} + M_{1C} + M_{1C} + M_{1C}) \times 0.03 - 4 \times (373+373) \times 0.03 \geq 479 \text{ kN·m}$$

Constraint equation based on mechanism in Fig. 15(f) – Strong column and weak beam

$$4 \times (M_{1C} + M_{1C} + M_{1B} + M_{1B}) \times 0.03 \geq 479 \text{ kN·m}$$

Additional constraint equation at joints – code requirement

$$M_{1C} + 373 - M_{1B} \geq 0$$

Objective Function – Weight, W

$$W = 4.627\, M_{1C} + 4.627\, M_{1C} + 7.315\, M_{1B}$$

Mathematical formulation of the minimization problem

Minimize:

$$W = 8.534\, M_{1C} + 7.315\, M_{1B}$$

Subject to:

$$0.48\, M_{1C} \geq 569 \text{ kN·m}$$

$$0.24\, M_{1C} + 0.24\, M_{1B} \geq 479 \text{ kN·m}$$

$$M_{1C} - M_{1B} \geq 0$$

$$M_{1B} \geq 0.60\, M_{1C}$$

where $M_{1B} > 0,\ M_{1C} > 0$

The optimized solution obtained using the simplex linear solver built in Microsoft Excel is

$$M_{1C} = 1186 \text{ kN·m and } M_{1B} = 812 \text{ kN·m}$$

Step 7: Effect of axial force on plastic capacity demands

To account for the reduction in the plastic moment capacities of columns due to the presence of an axial compression force as a result of the simultaneous actions of gravity and lateral loads during a seismic event, Eq. (29) is used to amplify the plastic moment demands. The term P_r/P_c used to calculate the amplification factor β_m is obtained as the ratio of the applied axial force during a seismic event to the axial compression capacity of the member under consideration. In line with the load proportions considered while determining the seismic mass, the axial force is assumed to be consisted of 100% and 25% of the applied dead and the live loads, respectively.

Story	Column size	Axial force (kN)		β_m	Plastic moment (kN·m)	
		Capacity	Applied		Required	Modified
1	W14×90	4306	565	1.070	1185	1268
2	W14×90	4484	365	1.042	373	389
3	W14×90	4484	165	1.019	57	58.5

Step 8: Plastic moment capacity versus demand comparison

The last step for each iteration in the proposed EBSD procedure is the selection of new member sizes that meet the required plastic moment capacity obtained in Step 7. When selecting new member sizes for columns, it is important to avoid the possibility of weak or extremely strong story with respect to the story immediately above it. At this step the plastic moment capacities of current member sizes are compared with the required plastic moment capacities based on the energy-based seismic design. If the plastic moment required is less than the plastic moment capacity of the current member size, then the current size remains unchanged. For multistory frames, the required column member sizes can be excessively large at the end of the first iteration and need to be optimized in successive iterations. The plastic moment demand-capacity comparison and selection of new member sizes as required are tabulated below.

	Story	Current size	Plastic moment (kN·m)		Member size	
			Capacity	Required	Decision	New
Columns	1	W14×90	856	1268	Change	W14×132
	2	W14×90	856	389	Keep	W14×90
	3	W14×90	856	58.5	Keep	W14×90
Beams	1	W18×76	920	812	Keep	W18×76
	2	W18×76	920	224	Keep	W18×76
	3	W18×76	920	57.4	Keep	W18×76

Another iteration is then carried out, and the results of this iteration are given below.

	Story	Current Size	Plastic moment (kN·m)		Member size	
			Capacity	Required	Decision	New
Columns	1	W14×132	1322	1182	Keep	W14×132
	2	W14×90	856	444	Keep	W14×90
	3	W14×90	856	74	Keep	W14×90
Beams	1	W18×76	920	698	Keep	W18×76
	2	W18×76	920	256	Keep	W18×76
	3	W18×76	920	72	Keep	W18×76

Because the current member sizes have more capacity than what the demand calls for, no further iterations are needed. The current sizes can be taken as the final design sections.

10 Summary and conclusion

To apply energy-based seismic design procedures to MDOF systems, the input and hysteretic energy spectra developed for SDOF systems need to be extended. In this paper, a procedure for estimating input and hysteretic energies for MDOF systems from equivalent SDOF systems was proposed and verified. Furthermore, a distribution scheme for distributing the hysteretic energy over the height of a multistory steel moment frame was proposed. The proposed scheme is based on work done by the modal forces as they act through the corresponding story displacements, and requires the designer to compute the modal forces for each mode using any existing procedure, apply these forces to the frame, and calculate the displacements due to these modal forces. A comparison of this proposed hysteretic equation with the actual hysteretic energy distribution from a pushover analysis showed that the proposed equation gave rather good results.

An energy-based seismic design procedure applicable for the design of steel moment-resisting frames was outlined. The procedure calls for the use of plastic steel design concept in conjunction with an optimization scheme applied to the frame in a story-wise manner to arrive at an acceptable design. In the context of this paper, an acceptable design is one in which the selected members not only have sufficient energy absorbing capacities to overcome the hysteretic energy demand but they are also the lightest. A design example was used to demonstrate the working of the proposed procedure.

Energy-based seismic design (EBSD) is considered a more rational design method because it deals directly with energy, not just force or displacement. The proposed design method is made possible by (1) developing input and hysteretic-to-input energy spectra for different soil site classes, different hysteretic models, and a range of ductility most often encountered for real structures (Mezgebo and Lui (2016); (2) relating the input and hysteretic energies for MDOF and equivalent SDOF systems; (3) proposing a hysteretic energy distribution scheme for multi-story frame; and (4) recommending a design procedure for applying the EBSD procedure to steel moment-resisting frames. Although the current design procedure is applicable only to steel moment-resisting frames, the implementation of the procedure to other frame types is possible once the energy absorbing mechanisms of such frames are identified and equations to quantify the absorbed energy for these frames are developed.

References

Akbas B, Shen J and Hao H (2001), "Energy Approach in Performance-based Seismic Design of Steel Moment Resisting Frames for Basic Safety Objective," *Structural Design of Tall Buildings*, **10**(3): 193–217.

Akiyama H (1985), *Earthquake-resistant Limit State Design for Buildings*, University of Tokyo Press, Tokyo, Japan.

ANSI/AISC 360-10 (2010), *Specification for Structural Steel Buildings*, American Institute of Steel Construction, Chicago, IL.

ATC 40 (1996), *Seismic Evaluation and Retrofit of Concrete Buildings*, Applied Technology Council, Redwood City, CA.

Benavent-Climent A (2011), "An Energy-based Method for Seismic Retrofit of Existing Frames Using Hysteretic Dampers", *Soil Dynamics and Earthquake Engineering*, **31**: 1385–1396.

BISPEC (2012), *Earthquake Solutions*, www.eqsols.com.

Chopra AK (2012), *Dynamics of Structures – Theory and Applications to Earthquake Engineering*, 4th ed, Pearson, Upper Saddle River, NJ.

Chopra AK and Goel RK (2002), "A Modal Pushover Analysis Procedure for Estimating Seismic Demands for Buildings," *Earthquake Engineering and Structural Dynamics,* **31**(3): 561–582.

Chou CC (2001), *An Energy-based Seismic Evaluation Procedure for Moment-resisting Frames*, Doctoral

Dissertation, Department of Structural Engineering, University of California-San Diego, La Jolla, CA.

Chou CC and Uang CM (2003), "A Procedure for Evaluating Seismic Energy Demand of Framed Structures," *Earthquake Engineering and Structural Dynamics*, **32**(2): 229–244.

Disque RO (1971), *Applied Plastic Design in Steel*, Van Nostrand Reinhold, NY.

Estes KR and Anderson JC (2004), "Earthquake Resistant Design Using Hysteretic Energy Demands for Low-rise Buildings," *Proceedings of the 13th World Conference on Earthquake Engineering,* Vancouver, B.C., Canada.

Fajfar P, Vidic T and Fischinger M (1989), "Seismic Design in Medium- and Long-period Structures," *Earthquake Engineering and Structural Dynamics*, **18**(8): 1133–1144.

FEMA 267A (1997), *Interim Guidelines Advisory No. 1,* Federal Emergency Management Agency, Washington, D.C.

FEMA 273 (1997), *NEHRP Guidelines for the Seismic Rehabilitation of Buildings*, Federal Emergency Management Agency, Washington, D.C.

FEMA 350 (2000), *Recommended Seismic Design Criteria for Steel Moment-frame Buildings*, Federal Emergency Management Agency, Washington, D.C.

Foti D, Bozzo LM and López Almansa F (1998), "Numerical Efficiency Assessment of Energy Dissipators for Seismic Protection of Buildings," *Earthquake Engineering & Structural Dynamics*, **27**: 543–556.

Gupta A and Krawinkler H (1999), *Seismic Demands for Performance Evaluation of Steel Moment Resisting Frame Structures*, Report No. 132, John A. Blume Earthquake Engineering Center, Stanford University, Stanford, CA.

Hernandez-Montes E, Kwon O and Aschheim MA (2004), "An Energy Based Formulation for First and Multiple Mode Nonlinear Static (Pushover) Analysis," *Journal of Earthquake Engineering*, **8**(1): 69–88.

Housner GW (1956), "Limit Design of Structures to Resist Earthquakes," *Proceedings of the 1st World Conference on Earthquake Engineering*, California, 1-13.

IBC (2012), *International Building Code*, International Code Council, Country Club Hills, IL.

Kuwamura H and Galambos TV (1989), "Earthquake Load for Structural Reliability," *Journal of Structural Engineering*, ASCE, **115**(6): 1446–1462.

Li HN, Wang F and Lu Z H (2007), "Estimation of Hysteretic Energy of MDOF Structures Based on Equivalent SDOF Systems" *Key Engineering Materials*, **340**: 425–440.

Liang Z, Lee GC, Dargush GF and Song J (2012), *Structural Damping – Applications in Seismic Response Modification*, CRC Press, Boca Raton, FL.

Manoukas G, Athannatopoulou A and Avramidis I (2011), "Static Pushover Analysis Based on Energy Equivalent SDOF System," *Earthquake Spectra*, **27**(1): 89–105.

Mezgebo MG and Lui EM (2016), "Hysteresis and Soil Site Dependent Input and Hysteretic Energy Spectra for Far-sourced Ground Motions," *Advances in Civil Engineering*, Vol. 2016, Article ID 1548319, http://dx.doi.org/10.1155/2016/1548319

Nakashima M, Saburi K and Tsuji B (1996), "Energy Input and Dissipation Behavior of Structures with Hysteretic Dampers," *Earthquake Engineering and Structural Dynamics*, **19**(1): 77–90.

Perform 3-D (2011), Computers and Structures, www.csiamerica.com/products/perform-3d.

Prasanth T, Siddhartha G. and Kevin RC (2008), "Estimation of Hysteretic Energy Demand Using Concepts of Modal Pushover Analysis," *Earthquake Engineering and Structural Dynamics*, **37**(6): 975–990.

Ridha RA and Wright RN (1967), "Minimum Cost Design of Frames," *Journal of Structural Division,* ASCE, **93**(4): 165–183.

SAP 2000 (2014), Computers and Structures, http://www.csiamerica.com/products/sap2000.

Seneviratna GDPK and Krawinkler H (1997), *Evaluation of Inelastic MDOF Effects for Seismic Design*, Report No. 120, John A. Blume Earthquake Engineering Center, Stanford University, Stanford, CA.

Shen J and Akbas B (1999), "Seismic Energy Demand in Steel Moment Frames," *Journal of Earthquake Engineering*, **3**(4): 519–559.

Terapathana S (2012), *An Energy Method for Earthquake Resistant Design of RC Structures*, Doctoral Dissertation, University of Southern California, Los Angeles, CA.

Uang CM and Bertero VV (1990), "Evaluation of Seismic Energy in Structures", *Earthquake Engineering and Structural Dynamics*, **19**(1): 77–90.

UBC (1997), *Uniform Building Code*, International Conference of Building Officials, Whittier, CA.

Wang F and Yi T (2012), "A Methodology for Estimating Seismic Hysteretic Energy of Buildings," *ASCE 2012 International Conference on Civil Engineering and Urban Planning*, Yantai, China, 17–21.

Ye L, Cheng G and Qu X (2009), "Study on Energy Based Seismic Design Method and the Application for Steel Braced Frame Structures", *Sixth International Conference on Urban Earthquake Engineering*, Tokyo Institute of Technology, Tokyo, Japan, 417–428.